

Potential Biosignatures in Super-Earth Atmospheres II. Photochemical Responses

J.L. Grenfell,^{1,§} S. Gebauer,¹ M. Godolt,^{1,§} K. Palczynski,^{1,*} H. Rauer,^{1,2} J. Stock,^{2,#}
P. von Paris,^{4,§} R. Lehmann,³ and F. Selsis⁴

Abstract

Spectral characterization of super-Earth atmospheres for planets orbiting in the habitable zone of M dwarf stars is a key focus in exoplanet science. A central challenge is to understand and predict the expected spectral signals of atmospheric biosignatures (species associated with life). Our work applies a global-mean radiative-convective-photochemical column model assuming a planet with an Earth-like biomass and planetary development. We investigated planets with gravities of 1g and 3g and a surface pressure of 1 bar around central stars with spectral classes from M0 to M7. The spectral signals of the calculated planetary scenarios have been presented in an earlier work by Rauer and colleagues. The main motivation of the present work is to perform a deeper analysis of the chemical processes in the planetary atmospheres. We apply a diagnostic tool, the Pathway Analysis Program, to explore the photochemical pathways that form and destroy biosignature species. Ozone is a potential biosignature for complex life. An important result of our analysis is a shift in the ozone photochemistry from mainly Chapman production (which dominates in Earth's stratosphere) to smog-dominated ozone production for planets in the habitable zone of cooler (M5–M7)-class dwarf stars. This result is associated with a lower energy flux in the UVB wavelength range from the central star, hence slower planetary atmospheric photolysis of molecular oxygen, which slows the Chapman ozone production. This is important for future atmospheric characterization missions because it provides an indication of different chemical environments that can lead to very different responses of ozone, for example, cosmic rays. Nitrous oxide, a biosignature for simple bacterial life, is favored for low stratospheric UV conditions, that is, on planets orbiting cooler stars. Transport of this species from its surface source to the stratosphere where it is destroyed can also be a key process. Comparing 1g with 3g scenarios, our analysis suggests it is important to include the effects of interactive chemistry. Key Words: Exoplanets—Earth-like—M-dwarf—Photochemistry—Biosignatures. *Astrobiology* 13, 415–438.

1. Introduction

UNDERSTANDING the photochemical responses of super-Earth (SE) atmospheres in the habitable zone (HZ) of M dwarf stars is a central goal of exoplanet science, since it is feasible that such environments may present the first opportunities to search for biosignature spectral signals. Gliese 581d (Udry *et al.*, 2007; Mayor *et al.*, 2009) is the first SE to be found that may orbit in the HZ of its M dwarf star. Recently, initial constraints on the composition of hot transiting SEs such as CoRoT-7b (*e.g.*, Guenther *et al.*, 2011) and GJ1214b (*e.g.*, Bean *et al.*, 2011; Croll *et al.*, 2011) have been discussed. Kepler 22b

(Borucki *et al.*, 2012) is the first transiting object found to occur in the HZ of a Sun-type star, several Earth-sized objects have been found orbiting a cool M dwarf (*e.g.*, Muirhead *et al.*, 2012), and detection of further SEs in the HZ is just beginning (*e.g.*, Bonfils *et al.*, 2013).

There exist a large number of possible parameters that could influence the abundances of possible biosignature species in hypothetical Earth-like atmospheres. Our motivation here is to take two parameters that are relatively well known, namely, stellar class and planetary gravity, and perform a sensitivity study assuming an Earth-like biomass and development in order to determine their effect upon the

¹Zentrum für Astronomie und Astrophysik, Technische Universität Berlin (TUB), Berlin, Germany.

²Institut für Planetenforschung, Deutsches Zentrum für Luft- und Raumfahrt (DLR), Berlin, Germany.

³Alfred-Wegener-Institut für Polar- und Meeresforschung, Potsdam, Germany.

⁴Université de Bordeaux and CNRS, LAB, UMR 5804, Floirac, France.

*Present address: Helmholtz-Zentrum Berlin für Materialien und Energie GmbH, Berlin, Germany.

[§]Now at Institut für Planetenforschung, Deutsches Zentrum für Luft- und Raumfahrt (DLR), Berlin, Germany.

[#]Now at Instituto de Astrofísica de Andalucia, IAA-CSIC, Granada, Spain.

photochemistry and climate and hence the potential biosignatures. Other works (*e.g.*, Segura *et al.*, 2005; Grenfell *et al.*, 2007) have also adopted this approach.

In this work, we analyzed the photochemical responses of key species from the same scenarios as the earlier work of Rauer *et al.* (2011) (hereafter Paper 1), who analyzed spectral signals for Earth-like planets with gravities of 1g and 3g orbiting in the HZ of M dwarf stars with classes from M0 to M7. In an earlier study, Segura *et al.* (2005) also discussed photochemical responses of (1g) Earth-like planets orbiting in the HZ of M dwarf stars. They calculated enhanced abundances of methane (CH₄) (by about 100×) and nitrous oxide (N₂O) (by about 5×) compared with those of Earth related to the weaker UV emissions of M dwarf stars. Their results also suggest a reduction in the ozone (O₃) column by up to about a factor of 7 compared with that of Earth, associated with weakened UV leading to a slowing in the O₃ photochemical source. This result was already broadly anticipated in the early 1990s (see Segura *et al.*, 2005, and references therein). In the present study, we aimed to examine the nature of these photochemical responses in more depth. We applied a diagnostic tool termed the Pathway Analysis Program (PAP) written by Lehmann (2004) to investigate the photochemical responses. PAP delivers unique information on chemical pathways of key species and has identified new chemical atmospheric pathways on Earth (Grenfell *et al.*, 2006) and on Mars (Stock *et al.*, 2012a, 2012b). PAP is a key tool for understanding atmospheric sources and sinks of the biosignatures and related compounds. The usual mechanisms that operate in Earth's atmosphere (*e.g.*, O₃ catalytic cycles) are complex and may be very different for Earth-like planets orbiting M dwarf scenarios, which is a good motivation for applying such a tool.

The primary driver of the photochemistry is the top-of-atmosphere (TOA) stellar flux, especially in the UVB and UVC regions, which weaken with decreasing effective stellar temperature. Therefore, we first analyzed the UV fluxes in our planetary atmospheres. Then, we focused on their influence on atmospheric ozone (O₃), since this is not only an important biosignature but also a key UVB absorber governing the abundances of other chemical species. We then investigated the biomarker N₂O, which is sensitive to UVB. Finally, we analyzed the photochemistry of CH₄ and water (H₂O), since these key greenhouse gases can influence surface habitability. We now present a brief overview of the photochemistry of the above four species.

1.1. Photochemistry of O₃

O₃ on Earth is a potential biosignature associated mainly with molecular oxygen (O₂), which arises mostly via photosynthesis. In Earth's atmosphere, about 90% (10%) of O₃ resides in the stratosphere (troposphere). Production of O₃ in Earth's stratosphere occurs mainly via the Chapman mechanism (Chapman, 1930) via O₂ photolysis. Production of O₃ in the troposphere occurs mostly via the smog mechanism (Haagen-Smit, 1952), which requires volatile organic compounds, nitrogen oxides, and UV.

Destruction of O₃ in the stratosphere proceeds mainly via catalytic cycles involving hydrogen oxides, nitrogen oxides, or chlorine oxides (*e.g.*, Crutzen, 1970) (designated HO_x, NO_x, and ClO_x, respectively). These molecules can be stored

in so-called reservoir species, the atmospheric distributions of which are reasonably well defined for Earth [*e.g.*, World Meteorological Organization (WMO) report, 1995]. Changes in, for example, temperature and/or UV can lead to the reservoirs releasing their HO_x-NO_x-ClO_x, associated with rapid stratospheric O₃ removal in sunlight. Destruction of O₃ in the troposphere occurs, for example, via wet and dry deposition and/or gas-phase removal via fast removal with, for example, NO_x.

O₃ can be formed abiotically in CO₂ atmospheres (*e.g.*, Segura *et al.*, 2007). O₃ layers (albeit very weak compared to that on Earth) have been documented on Mars (Fast *et al.*, 2009) and on Venus (Montmessin *et al.*, 2011), so caution is warranted when interpreting O₃ signals as indicative of biology or not (*e.g.*, Selsis *et al.*, 2002).

1.2. Photochemistry of N₂O

N₂O is a biosignature produced almost exclusively on Earth from microbes in the soil as part of the nitrogen cycle (Houghton *et al.*, 2001). Minor inorganic sources include, for example, the reaction of molecular nitrogen with electronically excited atomic oxygen: N₂ + O(¹D) + M → N₂O + M (*e.g.*, Estupiñan *et al.*, 2002). Destruction of N₂O occurs in the stratosphere mainly via photolysis or via removal with excited oxygen atoms.

1.3. Photochemistry of CH₄ and methyl chloride (CH₃Cl)

CH₄ is a strong greenhouse gas affecting climate and hence habitability. It is destroyed in the troposphere up to the mid stratosphere mainly by oxidative degradation pathways with hydroxyl (OH) and in the upper stratosphere via photolysis. CH₄ is a possible indicator of life (bioindicator) but not a definite proof, since this species (on Earth) has, in addition to biogenic sources, some geological origins (Houghton *et al.*, 2001).

CH₃Cl on Earth has important biogenic sources associated with vegetation, although its source-sink budget and net anthropogenic contribution are not well known (Keppler *et al.*, 2005). Like CH₄, its removal is controlled by reaction with OH, although the chlorine atom leads to increased reactivity (with an enhanced rate constant of about a factor of 6 for this reaction) compared with CH₄.

1.4. Photochemistry of H₂O

Although not a biosignature, H₂O is essential for life as we know it. Like CH₄, H₂O is an efficient greenhouse gas. Production of H₂O in Earth's stratosphere proceeds via CH₄ oxidation, whereas destruction of H₂O occurs in the upper stratosphere via photolysis (WMO, 1995). In the troposphere, H₂O is subject to the hydrological cycle, including evaporation and condensation.

1.5. Key questions

O₃ is formed on Earth in different ways, that is, via the smog mechanism (~10% on Earth) and the Chapman mechanism (~90%). How and why these values may change for different exoplanetary scenarios is not well investigated, yet this is important information for predicting and interpreting spectra. A flaring M dwarf star, for example, will

induce a photochemical response creating NO_x , which destroys “Chapman”-produced O_3 but could actually enhance a “smog” O_3 signal.

N_2O is destroyed via photolysis in the stratosphere by UVB radiation in the stratosphere, but its supply upward from the surface is controlled by atmospheric transport and mixing. Models with fast upward transport will ultimately lead to reduced N_2O abundances since, in the case of faster transport, the N_2O molecules reach the altitudes of efficient destruction earlier; that is, the lifetime of N_2O molecules is reduced, which (at a constant emission rate) leads to smaller N_2O concentrations. To improve knowledge of potential N_2O spectral signals in exoplanetary environments, it is important to understand which processes (photochemistry or transport) dominate the abundance of N_2O in different environments. For example, N_2O on Earth is affected by stratospheric UVB (which depends on, *e.g.*, the solar spectra, radiative transfer, atmospheric photochemistry) as well as tropospheric-to-stratospheric transport processes.

To begin to address such questions, we apply a new chemical diagnostic tool, PAP, which sheds unique light into the chemical pathways that control biosignature abundances.

2. Models and Scenarios

2.1. Models

The model details for the atmospheric coupled climate-chemistry column model and the theoretical spectral model have been described in Paper 1. Recent model updates include, for example, a new offline binning routine for calculating the input stellar spectra and a variable vertical atmospheric height in the model; more details were given by Rauer *et al.* (2011). The radiative-convective module is based on the work of Toon *et al.* (1989) for the shortwave region and the Rapid Radiative Transfer Module for the thermal radiation. Since a main focus in this work is on photochemical effects, we will now provide a detailed description of the photochemical module. The model simulates 1-D global-average, cloud-free conditions, although the effects of clouds were considered in a straightforward way by adjusting the surface albedo until the mean surface temperature of Earth (288 K) was attained for the Earth control run, as in earlier studies (Paper 1; Segura *et al.*, 2003). The scheme solved the central chemical continuity equations by applying an implicit Euler solver that used the Lower Upper triangular matrix decomposition method with variable iterative stepping such that the step size was halved whenever the abundance of a long-lived species changed by more than 30% over a single step. The version used here employs chemical kinetic data from Jet Propulsion Laboratory Evaluation Number 14 (NASA Panel for Data Evaluation, 2003). The scheme includes the key inorganic gas-phase and photolytic chemical reactions commonly applied in Earth’s atmosphere, that is, with hydrogen-oxide, nitrogen-oxide, and chlorine-oxide reactions and their reservoirs. The scheme was considered to be converged when the relative change in concentration for any species in any layer changes by less than 10^{-4} over a chemical iteration that exceeded 10^5 s.

From a total of 55 chemical species, 34 were “long-lived,” that is, the transport timescales are long compared with those of the photochemistry. Their concentrations were calculated by solving the full Jacobian matrix; three species,

namely, CO_2 , N_2 , and O_2 , were set to constant isoprofile values based on modern Earth, and the remainder of the species were “short-lived,” that is, assumed to be in steady state and therefore calculated from the long-lived species. The steady-state assumption simplifies the numerical solution.

Surface biogenic and source gas fluxes for CH_4 (531 Tg/yr), N_2O (8.6 Tg N contained in N_2O /yr), CO (1796 Tg/yr), and CH_3Cl (3.4 Tg/yr) were set such that for the Earth control run, Earth’s modern-day concentrations were achieved at the surface—this procedure was commonly used in earlier approaches for Earth-like exoplanets (*e.g.*, Paper 1; Segura *et al.*, 2003). H_2 at the surface was removed with a constant deposition velocity of 7.7×10^{-4} cm s^{-1} . Dry and wet deposition removal fluxes for other key species were included via molecular velocities and Henry’s law coefficients, respectively. Volcanic fluxes of SO_2 and H_2S were based on modern Earth. Tropospheric lightning sources of NO were based on the Earth lightning model of Chameides *et al.* (1977), assuming chemical equilibrium between N_2 , O_2 , and NO, a freeze-out temperature of 3500 K, and equilibrium constants taken from the Chemical Rubber Company (CRC, 1976) handbook. Modern Earth’s atmosphere has ~ 44 lightning flashes per second global mean (with flashes mainly generated over land in the tropics), which produces ~ 5 Tg N in the form of NO_x globally per year (Schumann and Huntreiser, 2007). Clearly, these values depend, for example, on atmospheric transport, convective activity, and the land-sea distribution for Earth-like exoplanets, which are not well-constrained parameters. At the model upper boundary, a constant, downward (effusion) flux of CO and O is set, which represents the photolysis products of CO_2 that are formed above the model’s upper lid.

Atmospheric mixing between the 64 vertical chemical layers was calculated via eddy diffusion constants (K in $\text{cm}^2 \text{s}^{-1}$), where $\log(K)$ varied from ~ 5.0 at the surface, decreased to a minimum value of ~ 3.6 at ~ 16 km, and then increased to ~ 5.7 at the model upper boundary.

Photolysis rates included the major absorbers, including important (E)UV absorbers such as O_2 , CO_2 , H_2O , O_3 , NO, CH_4 , and SO_2 . The O_2 photolysis absorption coefficients were calculated with the mean exponential sums method. The O_3 coefficients included the Hartley-Huggins T dependence based on data measured at 203 and 273 K (and linearly interpolated between). Species that photolyze in the UVB that are relevant for O_3 destruction were also included; for example, nitric acid (HNO_3) photolysis was included—this is important for NO_x release. Finally, weakly bound species that photolyze in the UVA/visible region, for example, NO_3 , N_2O_5 , were included. Photolysis rates were calculated based on insolation fluxes from the delta two-stream module (Toon *et al.*, 1989). One hundred eight wavelength intervals were included from 175.4 to 855 nm in the UV and visible, nine intervals in the EUV from 130 to 175 nm, and one Lyman-alpha interval at 121.6 nm. Rayleigh scattering for N_2 , O_2 , and CO_2 was included.

The Pathway Analysis Program (PAP) was developed by Lehmann (2004) and applied by Grenfell *et al.* (2006) to Earth’s stratosphere and by Stock *et al.* (2012a, 2012b) to the martian atmosphere. In the present work, it is applied to SE planetary atmospheres. The PAP algorithm identifies and quantifies chemical pathways in chemical systems. Starting with individual reactions as pathways, PAP constructs

longer pathways step by step. To achieve this, short pathways already found are connected at so-called “branching point” species, whereby each pathway that forms a particular species is connected with each pathway that destroys it. Branching point species are chosen based on increasing lifetime with respect to the pathways constructed so far. In this work, all species with a chemical lifetime shorter than the chemical lifetime of the species being studied (*i.e.*, the biosignatures O₃, N₂O, and the greenhouse gas CH₄) are treated as branching point species. Since in general the chemical lifetime of all species varies with altitude, the choice of branching point species adapts to the local chemical and physical conditions. A detailed description of the PAP algorithm is given by Lehmann (2004). To avoid a prohibitively long computational time, pathways with a rate smaller than a user-defined threshold [in the present study, $f_{\min} = 10^{-8}$ parts per billion by volume per second (ppbv/s)] are deleted. The chosen $f_{\min} = 10^{-8}$ ppbv/s is sufficient for finding the 5 dominant pathways (*e.g.*, of N₂O, CH₄ loss) as shown in the tables (Appendix A1). Stock *et al.* (2012a) discussed the effect of varying this parameter. PAP calculates the chemical pathways by taking as input (i) a list of chemical species, (ii) chemical reactions, (iii) time-averaged concentrations and reaction rates, and (iv) concentration changes arising from the gas-phase chemical reactions only (*i.e.*, not including changes in abundance from, *e.g.*, mixing, deposition). PAP calculates as output the identified chemical pathways with their associated rates. Information from PAP is used to interpret chemical responses.

2.2. Scenarios

Here, we analyze the model scenarios described in Paper 1. We considered planets with masses corresponding to 1g and 3g with Earth-like (*i.e.*, N₂-O₂) atmospheres with Earth’s source gas emissions and initial p , T , and abundance profiles as for modern Earth. There are currently no observational constraints for the surface pressure of SE planets. On one hand, theoretical studies, for example, that of Elkins-Tanton and Seager (2008), have suggested a wide range of possible atmospheric masses resulting from outgassing on SE planets. On the other hand, for example, Stamenković *et al.* (2012), who included a pressure dependence of viscosity in the mantle, suggested rather weak SE outgassing rates. Given the current uncertainties, we therefore assume 1 bar surface pressure to be comparable with Paper 1 and earlier studies and to compare with our 1g scenarios. Our modeled p , T , and chemical output profiles are calculated self-consistently for planets around different central M dwarf stars in the HZ (with the Sun-Earth case for comparison). We explore an extensive parameter range, considering planets orbiting M dwarf stellar classes from M0 to M7. This is necessary because atmospheric chemistry-climate coupling is strongly nonlinear; hence, general results from one set of stellar classes (*e.g.*, M0–M4) cannot be simply extrapolated to other stellar classes (*e.g.*, M5–M7)—instead each scenario has to be calculated separately. Mixing ratios for radiative species are fed back into the climate module, which calculates a new T , p profile, and this is again fed back into the chemistry module. This iterative process continues until T , p , and concentrations all converge. The planets are placed at an orbital distance from their star such that the total energy input at the TOA

equals the modern solar constant of 1366 W m⁻² (see Paper 1 for the stellar input spectra used). In total, the following 11 scenarios were investigated:

1g Sun	(run 1)	Earth
3g Sun	(run 2)	Super-Earth with 3 times Earth’s gravity (3g) orbiting the Sun
1g M0	(run 3)	Earth-like planet (1g) orbiting M0 star
3g M0	(run 4)	Super-Earth (3g) orbiting M0 star
1g M4	(run 5)	Earth-like planet (1g) orbiting M4 star
3g M4	(run 6)	Super-Earth (3g) orbiting M4 star
1g ADL	(run 7)	Earth-like planet (1g) orbiting active AD Leonis (ADL)*
3g ADL	(run 8)	Super-Earth (3g) orbiting active AD Leonis
1g M5	(run 9)	Earth-like planet (1g) orbiting M5 star
3g M5	(run 10)	Super-Earth (3g) orbiting M5 star
1g M7	(run 11)	Earth-like planet (1g) orbiting M7 star

*Segura *et al.* (2005) and Rauer *et al.* (2011) adopted a spectral class of 4.5 based on the SIMBAD database, whereas Hawley and Pettersen (1991) used a value of 3.5.

2.3. Planetary radiation environment

2.3.1. Incoming stellar fluxes (F_{*}). These are the primary driver of planetary atmospheric photochemistry, especially in the UVB and UVC range, and are also central to habitability for life as we know it on Earth. A significant proportion of cooler M dwarfs like those considered in our work may be active emitters of UV from their chromospheres or/and transition regions (see, *e.g.*, Walkowicz *et al.*, 2008; France *et al.*, 2013). This could have a considerable impact upon the planetary photochemistry, climate, and associated biosignatures. How efficiently the UV is absorbed throughout the atmospheric column is closely linked with the photochemical responses and, hence, determines the final abundances of the biosignature. We therefore start our analysis by investigating the planetary radiation environment. We discuss UV radiation at the TOA and at the planetary surface and present a validation of surface UV based on Earth observations.

2.3.2. Planetary TOA radiation analysis. We analyzed the planetary TOA F_* in the UVA, UVB, and UVC wavelength range for the different stellar scenarios in the top model layer. UVA corresponds to the model wavelength intervals from 315 to 400 nm; UVB corresponds to 280–315 nm; UVC corresponds to 175.4–280 nm.

To be comparable with Paper 1, we approximated the TOA stellar spectra for the M0 to M7 M dwarf stars as Planck functions [other than for the Sun, which is for solar mean conditions based on the work of Gueymard *et al.* (2004), and for ADL, for which measured UV spectra are available; see Paper 1]. The approach used in Paper 1 and, therefore, in this study as well was to employ Planck curve spectra that correspond to quiet M dwarf stars with little emitted UV fluxes. Recent results (Reiners *et al.*, 2012) suggest that >90% of hotter (M0–M2) M-dwarf stars sampled are *quiet*, whereas >50% of the cooler stars (M4 and cooler) are *active*. Clearly, we are well aware that smooth Planck functions do not include, for example, enhanced Lyman-alpha and UVC features, characteristic of cool M dwarf stars that may have very

active chromospheric and coronal regions. However, direct observations of stellar spectra for the cooler M dwarf stars (M5–M7) in the critical wavelength range ($\lambda < \text{UVA}$) in our photolysis scheme are presently not available; hence we prefer to adopt such a Planck-spectrum approach. Future work will study the effect of varying (E)UV characteristic emissions in the input spectra. Further, by comparing results from scenarios in which Planck curve spectra are used with those for active stars, we can isolate the photochemical effects in the planetary atmosphere of varying stellar activity. First, to get an overview, Table 1 compares ratios of UV emission for our considered M dwarf scenarios with the Sun.

Table 1 (row 1) suggests that our cool (M7) M dwarf would emit less than 1% of the UVA, UVB, and UVC radiation compared with the Sun. Comparing (row 2) the active ADL M-dwarf star with the Sun suggests that UVA, UVB, and UVC for the flaring star amount to only 1–7% of the total solar radiation

Figure 1a–1c shows the TOA UVA, UVB, and UVC net flux (W m^{-2}). Figure 1 shows an increase with increasing stellar effective temperature as expected. The active ADL flaring case is an especially strong emitter of UV due to its extremely active chromosphere. Modeled TOA UVB flux for Earth ($\sim 18.3 \text{ W m}^{-2}$) compares reasonably well with available observations (e.g., $16 \pm 3 \text{ W m}^{-2}$; Benestad, 2006).

2.3.3. Planetary surface radiation. In the chemistry module, the UVA and UVB net fluxes required for the photolysis scheme are calculated from the top layer downward via the two-stream module with Rayleigh scattering. Figure 2a–2b shows UVA and UVB net flux (W m^{-2}) at the planetary surface as calculated in the chemistry module of this work. UVC is essentially zero at the surface so is not shown in Fig. 2, and similarly for Fig. 3. Generally, Fig. 2a and 2b shows an increase in planetary surface UV radiation with higher stellar temperatures, as for the TOA cases shown in Fig. 1.

2.3.4. Comparison with Earth surface UV radiation. Global satellite observations from 1992 to 1994 (Wang *et al.*, 2000, their Fig. 6b) suggest observed UVB surface radiation for Earth of $\sim 1.4 \text{ W m}^{-2}$ for cloud-free conditions. By comparison, Fig. 2b suggests that our model overestimates this value, calculating 2.3 W m^{-2} UVB for the Earth control run. Uncertainties include, for example, our straightforward treatment of clouds, whereby we adjust the surface albedo (see above), as well as the challenge of representing, for example, time-dependent and, for example, latitude-varying O_3 photochemistry and UV absorption in a global-averaged 1-D model.

2.3.5. Ratio of surface to TOA UV flux. This ratio (R) is shown for the 1g and 3g cases in Fig. 3a and 3b for UVA and

TABLE 1. RATIOS OF UV RADIATION FOR OUR M DWARF STAR (M7) SCENARIO COMPARED WITH THE SUN (UPPER ROW) AND FOR ADL

Scenario	UVA	UVB	UVC
(M7/Sun)	5.1×10^{-3}	1.2×10^{-3}	3.2×10^{-4}
(M _{active} /Sun)	1.2×10^{-2}	1.2×10^{-2}	6.5×10^{-2}

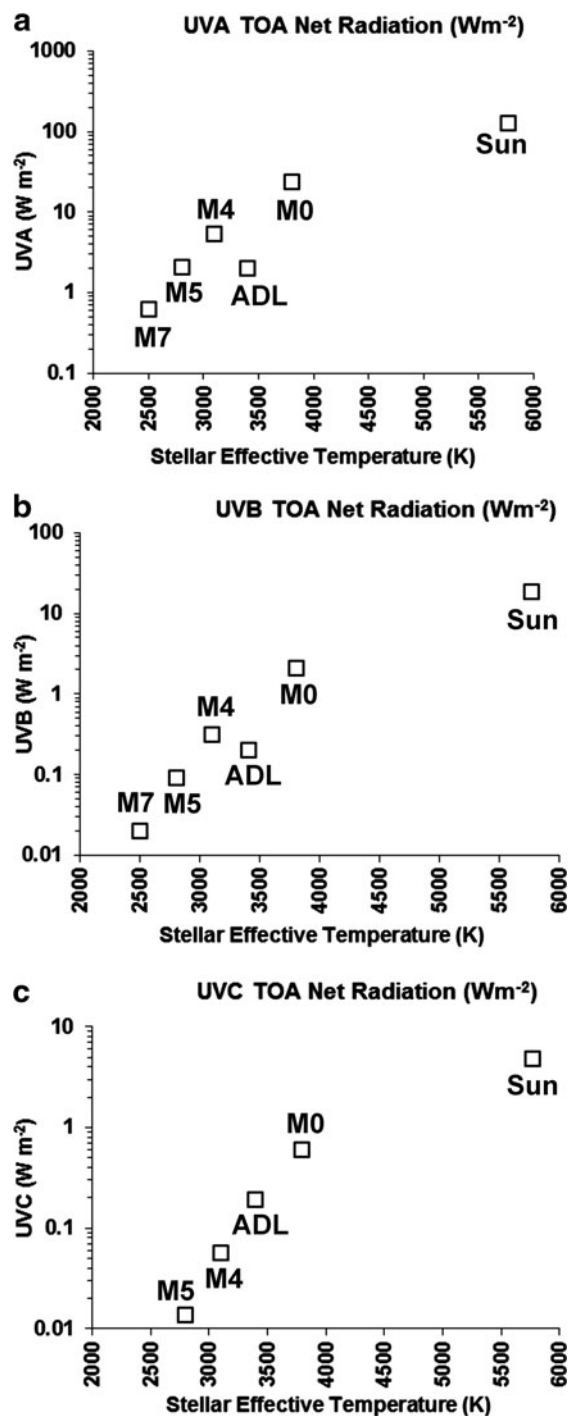


FIG. 1. Planetary global mean TOA incoming radiation (W m^{-2}) for UVA (a), UVB (b), and UVC (c) for Earth's gravity.

UVB, respectively. R is an inverse measure of the UV shielding of an atmosphere. Figure 3a suggests that UVA passes efficiently through the atmospheres considered, as expected, since most values of $R_{\text{net,UVA}}$ are > 0.7 . The UVA ratio is not greatly dependent on the stellar temperature.

Figure 3b shows as expected a much stronger atmospheric extinction of UVB than for the UVA wavelengths, and there is now a clear dependency on stellar temperature. Weaker overhead O_3 columns in the cool M dwarf cases lead to a

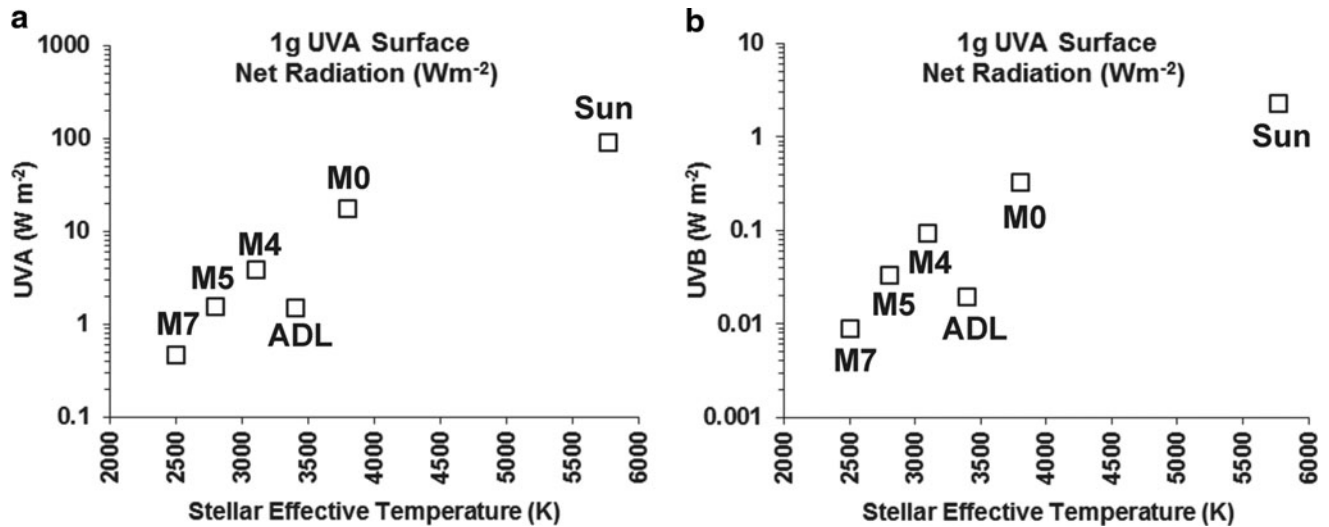


FIG. 2. As for Fig. 1 but at the planetary surface for UVA (a) and UVB (b) for Earth's gravity (1g).

strong rise in the ratio in Fig. 3b. For the 3g scenarios (circles), a lowering in the atmospheric column by a factor of three resulted in less UV shielding and a rise in the surface UV.

3. Chemical Analysis

Here, we first compare briefly previous results (Segura *et al.*, 2005) reported in the literature. Then, we discuss the general trends in column abundances of the biosignatures and related key species. Finally, we discuss the chemical responses for the vertical profiles that were also shown in Paper 1.

3.1. Column biomarkers (1g planets)

Column O₃ in Fig. 4a (blue diamonds) mostly decreased with increasing star class (*i.e.*, decreasing T_{eff} of the star) related to less UVB; therefore there was a slowing in the photolysis of molecular O₂ and hence a slowing in the Chapman cycle, a major source of O₃. The O₃ profile responses are discussed in more detail in Section 3.6. The column values are shown in Appendix Table A2.

Column N₂O in Fig. 4a (red squares) generally increased with increasing star class. The cooler stars emit less UVB, which suggests a slowing in the photolytic loss of N₂O in the planetary atmosphere and hence an increase in its abundance.

Column CH₃Cl in Fig. 4a (green triangles) generally increased with increasing star class due to less OH, its major sink (see OH analysis, Table 2). The response is comparable to CH₄ (discussed in the next section), which has a similar photochemistry. Spectral features of CH₃Cl, however, were too weak to be evident in the calculations of Paper 1 despite the enhanced column amounts for the cooler stars.

3.2. Column biosignatures (3g planets)

For the 3g planets, we assumed a constant surface pressure of 1 bar, which led to the total atmospheric column being reduced by a factor of 3, as already mentioned (Fig. 4b). The general trends for O₃ and N₂O remain for the 3g scenarios, that is, mostly similar to the corresponding 1g scenarios already discussed, although the reduced total

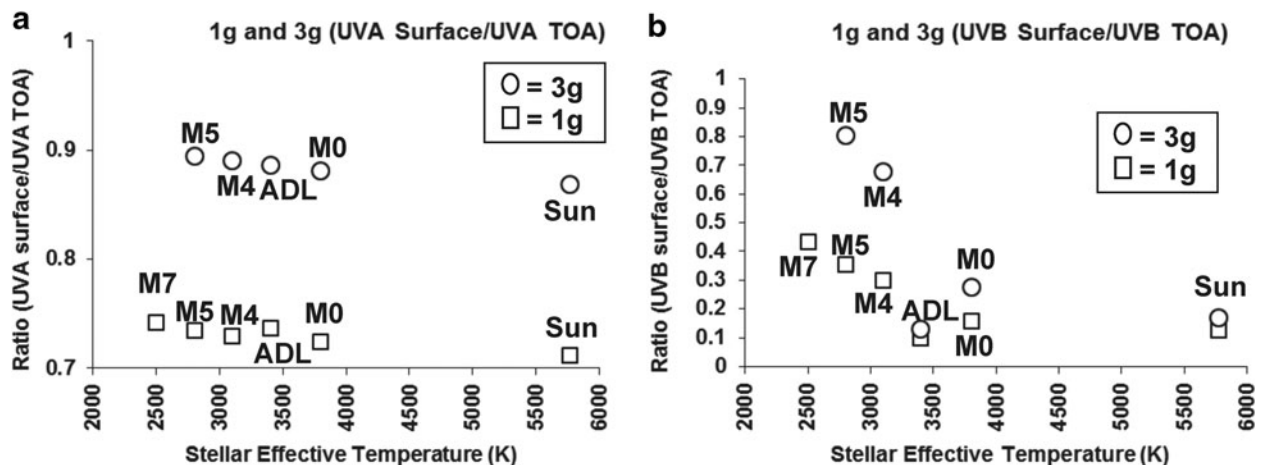


FIG. 3. As for Fig. 1 but showing the ratio (surface/TOA) (at 1g and 3g) for UVA (a) and UVB (b) radiation.

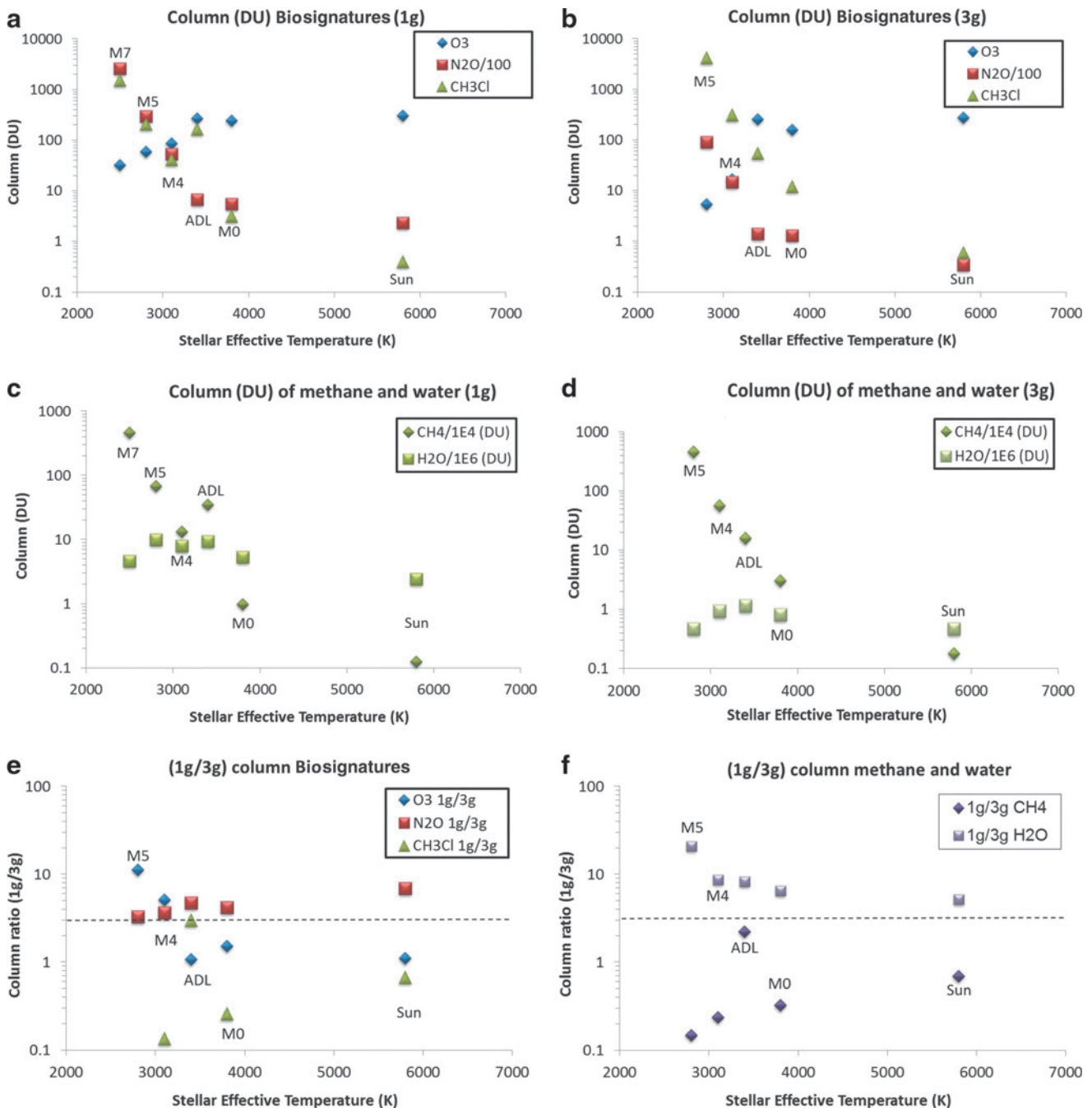


FIG. 4. (a) Atmospheric columns (Dobson units, DU) (1g) of biosignatures, ozone (O₃), nitrous oxide (N₂O), and methyl chloride (CH₃Cl). (b) As for (a) but for (3g) scenarios [same surface pressure (1 bar) as 1g]. (c) As for (a) but for column CH₄ (DU) and H₂O (DU). (d) As for (c) but for (3g) scenarios assuming same surface pressure (1 bar) as 1g cases. (e) Column (1g/3g) ratio for the same biosignatures as shown in (a). (f) Column (1g/3g) ratio for the same greenhouse gases as shown in (c). Color images available online at www.liebertonline.com/ast

column resulted in a cooling of the lower atmosphere due to a weaker greenhouse effect, as we will show (see Paper 1 also).

The N₂O 3g response is linked with enhanced UVB penetrating the reduced atmospheric column compared with 1g, which leads to more photolytic loss of N₂O. A transport effect also took place. For the 3g case (with its lower model lid due to less atmospheric mass and higher gravity), the upward tropospheric diffusion of N₂O was faster, for example,

by about 50% in the mid to upper troposphere than for the 1g case. This meant that N₂O for the 3g case could reach the stratosphere faster, where it would be rapidly photolyzed.

3.3. Column greenhouse gases (1g planets)

In this section, we discuss the planetary atmospheric column abundances of CH₄ and H₂O since they have a major impact on temperature via the greenhouse effect. Vertical

TABLE 2. MODELED (LOWEST ATMOSPHERIC LAYER) AND OBSERVED (SURFACE) GLOBAL-MEAN KEY SPECIES' ABUNDANCES (MOLECULES CM⁻³) AND REACTION RATES (MOLECULES CM⁻³ S⁻¹) AFFECTING CH₄ (AND H₂O) FOR VARIOUS 1g SCENARIOS

Quantity	1g Sun	1g M0	1g M4	1g M5	1g M7	1g ADL
OH	1.3×10 ⁶ (Obs. = 1.1×10 ⁶)*	1.0×10 ⁵	4.0×10 ³	2.8×10 ²	7.0	1.3×10 ²
OH Source reaction Rate _{(O(1D)+H₂O→2OH)}	3.4×10 ⁵	1.3×10 ⁵	6.6×10 ⁴	2.2×10 ⁴	4.1×10 ³	1.1×10 ⁴
OH recycling reaction Rate _(NO+HO₂→NO₂+OH)	2.3×10 ⁵	1.5×10 ⁵	7.1×10 ⁴	3.1×10 ⁴	1.0×10 ⁴	2.3×10 ⁴
(HO ₂ /OH)	2.1×10 ²	1.6×10 ³	2.7×10 ⁴	2.2×10 ⁵	3.1×10 ⁶	2.8×10 ⁵
(NO ₂ /NO)	2.6	16.2	56.1	98.4	132.1	84.8
O ₃	4.7×10 ¹¹	6.0×10 ¹¹	4.6×10 ¹¹	3.2×10 ¹¹	1.8×10 ¹¹	3.0×10 ¹¹

*From Lelieveld *et al.* (2002).

profiles will be discussed later and can also be found in Paper 1.

3.3.1. CH₄ column response. Since the only source of CH₄ in the model is fixed biomass surface emission, the CH₄ response for the various runs is controlled by the main atmospheric CH₄ sink, that is, removal via the hydroxyl (OH) radical. OH is affected by three main processes:

OH source(s): for example, H₂O+O(¹D)→2OH [where O(¹D) comes mainly from O₃ photolysis in the UV].

OH recycling reactions in which NO_x species can interconvert HO_x (defined here as OH+HO₂) family members via, for example, NO+HO₂→NO₂+OH.

OH sinks, for example, reaction with CH₄ and CO [see, *e.g.*, Grenfell *et al.* (1999) for an overview].

Figure 4c suggests a strong CH₄ (green diamonds) increase with decreasing effective stellar temperature. Cooler stars are weak UV emitters, which favors a slowing in the OH source reaction above. Note also that greenhouse warming by the enhanced CH₄ favors a damp troposphere (more evaporation) and, hence, all else being equal, would favor actually *more* OH (via more H₂O; see source OH reaction above). This is an opposing process, which our results suggest is not the dominant effect. So, for a given model, calculating accurately the *net* effect will depend, for example, on a good treatment of, for example, the hydrological cycle, which is challenging for a global column model. To aid in understanding the CH₄ response, which is controlled by OH, Table 2 summarizes the OH sources, sinks, recycling budget, and associated quantities.

3.3.2. OH abundances. Control run (1g Sun) OH abundances in Table 2 are within ~20% of global-mean observed OH proxies for Earth. Table 2 suggests a strong decrease in OH from left to right (*i.e.*, for decreasing stellar effective temperature), especially for the M7 case.

3.3.3. OH source reaction rates. The source reaction rate (Sun) in Table 2, that is, O(¹D)+H₂O→2OH, is about 12 times weaker than indicated by the Whalley *et al.* (2010) study, which investigates (Earth) clean-air, tropical northern-hemisphere daytime OH. The factor 12 difference reflects a lowering due to day-night averaging in our global mean model (which accounts for ~factor 2 of the difference in OH) and the fact that the Whalley study considered tropical

conditions. Concentrations of the trace specie O(¹D) in the control run (6×10⁻⁸ ppbv at 30 km) compared reasonably well with Earth observations (~3×10⁻⁸ ppbv, Brasseur and Solomon, 2005). Table 2 suggests that the source reaction rate decreases from left to right, which is consistent with the decrease in OH.

3.3.4. OH recycling reaction rates. Our (Sun case) recycling reaction was comparable with that of the Whalley *et al.* (2010) study to within about 50%. Earlier (Earth) modeling studies, for example, that of Savage *et al.* (2001), suggest that the OH recycling reaction dominates the source reaction even in quite clean air-masses (NO_x ~250 pptv and below), which is somewhat in contrast to this and the Whalley study. In Table 2, the recycling reaction rates (like the source reaction) also decrease from left to right, which favors the decrease in OH, although the change in the source reaction is the stronger effect. For cooler stars, the recycling reaction becomes increasingly important compared with the source reaction, and it dominates for the ADL and M7 cases.

3.3.5. HO_x and NO_x ratios. These ratios are sensitive markers of changes in HO_x and NO_x chemistry and hence affect, for example, O₃ cycles and CH₄. The ratios (HO₂/OH) and (NO₂/NO) in Table 2 increase strongly for the cooler stars. These ratios are strongly affected by the concentration of O₃, whose production via the Chapman mechanism (discussed in 3.5) weakens for the cooler stars. The ratios for the cooler stars are far from their "Earth" values, so the interactions between HO_x and NO_x are much perturbed. This is a hint that the usual mechanisms that operate on Earth (*e.g.*, O₃ catalytic cycles) may be very different for the cooler star scenarios—a good motivation for applying PAP as already mentioned.

3.3.6. Atmospheric response for AD Leonis. Although the 1g ADL scenario featured lower OH (Table 2) than for M5, ADL featured *lower* CH₄ (Paper 1) than M5. The upper layers (>60 km) of the 1g ADL run showed very rapid destruction of CH₄ via OH—about 5 times faster than for M5. This was consistent with the high Lyman-alpha output of ADL leading to faster HO_x enhancement via H₂O photolysis.

3.3.7. Water column response. Figure 4c suggests that the increased CH₄ columns (green diamonds), with

decreasing stellar effective temperature generally (except for M7), lead to higher H₂O columns (green squares). Generally, for the cooler star scenarios, (up to and including M5), more CH₄ greenhouse heating leads to more water evaporation in the troposphere; and in the stratosphere, faster CH₄ oxidation leads to faster H₂O production. However, for the M7 case (Fig. 4c), although CH₄ increased, surface temperature did not, which suggests a saturation in the CH₄ greenhouse from M5 to M7, where the lower atmosphere becomes optically thick at very high CH₄ abundances. Surface cooling from M5 to M7 is also seen in the temperature profiles in Paper 1 (their Fig. 3).

3.4. Column greenhouse gases (3g planets)

3.4.1. CH₄ and H₂O. Figure 4d has a similar format to Fig. 4c but instead shows results for the 3g (instead of 1g in 4c) scenarios. The basic response to decreasing the effective stellar temperature at 3g is similar to the 1g case; that is, results suggest a column rise in CH₄ and in H₂O but with a drop-off in the latter for the cooler stars. To gain more insight into the effect of changing gravity, upon CH₄, Table 3 shows the ratio (1g/3g) of the CH₄ column and for the near-surface atmospheric OH abundance.

Without calculating interactive photochemistry, a passive tracer would undergo a column reduction by a factor of 3 from 1g to 3g, because at constant surface pressure, increasing gravity by a factor of 3 leads to column collapse and a reduction in the overhead column by the same factor as the increase in gravity. In Table 3, therefore, a hypothetical, passive tracer (with no chemistry) would have a value of exactly 3. The actual (with chemistry) CH₄ column ratios (row 1), however, are all less than 3. The reduction is consistent with faster chemical loss at 1g than at 3g. To investigate this further, OH ratios are shown in Table 3 (row 2). They mostly (except ADL) increase for the cooler stars, suggesting a lowering in the 3g OH abundances compared with the corresponding 1g cases for the cooler stars. This is consistent with faster chemical loss at 1g. The reduction in OH for the 3g scenarios implies that, for example, the increase in UVB due to weaker shielding of some 3g atmospheres (*favoring* OH production) is outweighed by the (opposing) feedback where reduced greenhouse warming at 3g led to a drier troposphere [disfavoring OH, which is produced via O(¹D) + H₂O → 2OH].

This is confirmed by the water column (open circles in Fig. 4d), which suggests that the 3g compared with 1g (Fig. 4c) scenarios led to a weakening in the greenhouse effect and hence tropospheric cooling (as seen in Fig. 2 of Paper 1) and a general lowering in the H₂O column (due to more condensation) by around a factor of 10 (Fig. 4d) compared with the 1g case (Fig. 4c). In general, however, note that responses in

chemical abundances do not scale directly with the column reduction at 3g compared with 1g since the effects of, for example, photochemistry are important.

Figure 4e–4f shows the ratios (1g column/3g column) for biosignature and greenhouse gases, respectively. The main point is that the values can lie far from a value of 3 (which would be expected for a passive tracer). This shows that it is important to include the effects of interactive chemistry. For the biosignature O₃ there is some indication of an increase in the ratio shown in Fig. 4e for the cooler stars, which will be the subject of future study. For CH₃Cl (Fig. 4e) and CH₄ (Fig. 4f) (which both have similar OH removal chemistry) the trend is downward for the cooler stars. The H₂O (Fig. 4f) scenarios are relatively more damp (with values > 3) than for a purely passive tracer. This suggests more efficient production of H₂O from CH₄ for the cooler stars at 3g than at 1g, for example, due to more UV in the thinner, 3g atmospheres.

3.5. Column-integrated PAP results

Figure 5 shows output of O₃ cycles from PAP. The cycles (divided into production and loss cycles) found have been quantified according to the rate of O₃ production or loss through each particular cycle expressed as a percentage of the total rate of production or loss found by PAP (see also description of Appendix A1 below). Values are integrated over the model vertical domain. PAP analyses were performed for each of the 64 vertical column model chemistry levels, and the column-integrated values are shown in Fig. 5. The full cycles referred to in Fig. 5 can be found in the appendix.

3.5.1. Sun PAP analysis. Figure 5 confirms the expected result for O₃ production, that is, the Chapman mechanism dominates over the smog mechanism. For O₃ destruction, the column model suggests strong NO_x contributions in the lower stratosphere, although an Earth GCM study (Grenfell *et al.*, 2006) suggests a strong HO_x contribution there. This result could reflect the challenge of 1-D models of capturing 3-D variations in photochemistry. Also, the column model does not include industrial emissions, unlike the Earth 3-D model. The result should be explored in future comparisons between the column model and 3-D runs.

3.5.2. Column-integrated O₃ (1g) production. Figure 5a suggests a change from a mainly Chapman-based O₃ production for the 1g Sun and the warmer 1g M dwarf stars, switching to a slower, mainly smog-based O₃ production for the cooler stars (1g M5 and 1g M7). This was related to the decrease in UVB for the cooler star scenarios, since UVB is required to initiate the Chapman mechanism via photolysis of O₂.

3.5.3. Column integrated O₃ (1g) destruction. Figure 5a also suggests that the classical NO_x and HO_x cycles (see also Figs. 6 and 7) that operate mainly in the stratosphere were the most dominant O₃ loss pathways for the Sun and warmer M dwarf scenarios. For the cooler star scenarios, the enhanced CO concentrations led to a CO-oxidation cycle gaining in importance.

3.5.4. Column O₃ (3g). Behavior at 3g (Fig. 5b) was broadly similar to that at 1g, except at 3g *both* Chapman and

TABLE 3. RATIO (1g/3g) FOR THE CH₄ ATMOSPHERIC COLUMN AND FOR NEAR-SURFACE OH (MIDPOINT OF LOWERMOST GRIDBOX) FOR THE SUN COMPARED WITH M DWARF STAR SCENARIOS

Quantity	Sun	M0	M4	M5	ADL
CH ₄ _col_1g/CH ₄ _col_3g	0.7	0.3	0.2	0.1	2.2
OH_surf_1g/OH_surf_3g	1.1	3.7	8.5	47.8	0.2

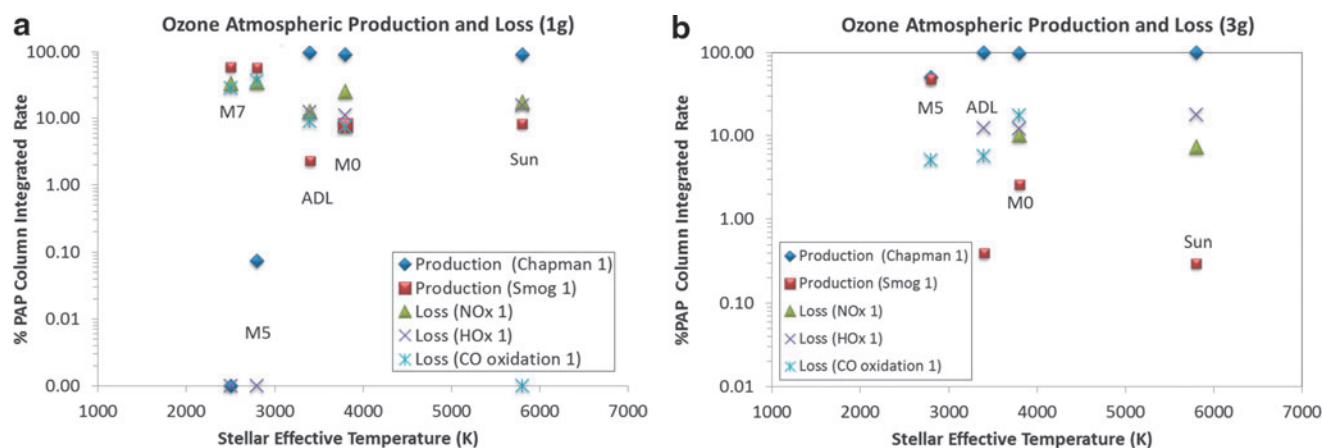


FIG. 5. Pathway analysis results for global mean ozone sources (a) and sinks (b) for the Sun and for the M dwarf star scenarios (1g) calculated by PAP. The pathways are shown in the PAP tables in the appendix. Color images available online at www.liebertonline.com/ast

smog were important O₃ producers for the M5 case (*i.e.*, not just smog as in the 1g case). Weaker atmospheric UVB absorption led to more penetration of UVB and hence an increased role for Chapman in the layers below.

3.5.5. Column-integrated results tables for O₃, N₂O, and CH₄. Appendix A1.1–A1.3 shows the integrated column mean PAP output for O₃, N₂O, and CH₄, respectively. Shown are (i) the column-integrated rates (CIR) (in molecules cm⁻² s⁻¹) for all pathways found by PAP (“Found_PAP”), (ii) the CIR for only the pathways shown in the appendix (“Shown_PAP”) (shown are either the five dominant pathways or the first pathways that together account for >90% of the total formation or loss of Found_PAP, whichever condition is fulfilled first), and (iii) the CIR as calculated in the chemistry scheme of the atmospheric column model (“Total_chem”). Percent values for a particular cycle show its individual rate as a percentage of Found_PAP.

Comparing these three CIR values, it can be seen that for the O₃ production, which is relatively straightforward, the pathways found by PAP can account very well for the rate calculated in the column model chemistry module. For the O₃ loss pathways, which are rather more complex than the production, PAP can still account for generally more than ~90% of the rate from the chemistry module. For the sometimes very complex CH₄ pathways, with the value of f_{\min} chosen for this study, PAP can account for only up to about 50% of the rate from the chemistry module. Further tests suggested that decreasing the PAP input parameter f_{\min} (the minimum considered flux, currently set to 10⁻⁸ ppbv/s for all runs) leads to improvement, but the resulting complex CH₄ cycles are beyond the scope of this paper (see also 3.6.3). We now discuss the individual cycles for each scenario.

3.5.6. O₃ Column-integrated pathways. Chemical pathways for the 1g Sun scenario in Appendix A1.1 mostly compare well with established results for Earth as discussed above. Appendix A1.1 suggests that for the 1g M0 scenario—due to less stellar UVB emission compared with the Sun—the Chapman mechanism for producing O₃ is somewhat suppressed (89.2%) and a new CO sink (“CO-oxidation 1”, 7.4%) appears, since CO is abundant. For the 3g M0 scenario, re-

sults suggest that Chapman features more strongly (96.7%) in the thinner 3g atmosphere compared with the corresponding 1g case. HO_x and NO_x remain important chemical sinks for both the 3g and 1g cases. The active star (1g ADL) features a stronger Chapman contribution (97.2%) compared with 1g M0 since ADL is especially active in the UV, which is important for Chapman initiation (via molecular oxygen) with only modest changes for the 3g ADL case. For cooler non-active stars (1g M5), large changes are apparent compared with the warmer star cases. Less UVB emission from the cool M5 star leads to a switch to smog-type O₃ production (“Smog 1”, 57.8%). As discussed, the atmosphere is abundant in CH₄ and CO. Thus, the “CO-oxidation 1” cycle is an important O₃ loss pathway (36.8%). For the 3g M5 case, the thinner total column at 3g compared with 1g leads to a rise in UV, which is consistent with more Chapman O₃ (47.8%) production than the 1g case (7.5%). For O₃ loss, a complex CH₄ oxidation pathway involving CH₃OOH becomes important (46.8%), which is not evident at 1g. The changed UV environment leads to a modest rise in HO_x in the upper troposphere at 3g. Finally, for the coolest M dwarf case (1g M7), O₃ production occurs via numerous types of smog mechanisms involving the oxidation of different volatile organic compounds, for example, CO, HCHO, and CH₃OOH. CO smog cycles become a key means of producing O₃ especially for the cooler stars. Like CH₄, an important sink for CO is the reaction with OH. As discussed, weakening UV emissions for the cooler stars leads to less OH and therefore an enhanced abundance of CO. Near the surface, CO mixing ratios correspond to 0.09 (Sun), 9.0 (M4), 64 (ADL), and 426 (M7) ppm. O₃ loss also involves NO_x cycles but also a smog mechanism (“Smog 7”) where O₃ is the net oxidant, which is consumed to oxidize CH₄ and a CO oxidation cycle.

Smog cycles have larger rates for the M5 and M7 scenarios than for the Sun and M0 scenarios. This is because the important “Smog 1” cycle (producing O₃) is in competition with the “CO-oxidation 1” pathway (destroying O₃). At high O₃ concentrations (for the Sun and M0 scenarios), (i) the reaction NO + O₃ → NO₂ + O₂ shifts the NO_x family to favor NO₂. The reduction in NO leads to a slowing in the key reaction NO + HO₂ → NO₂ + OH and hence slows the “Smog 1” cycle. Also at

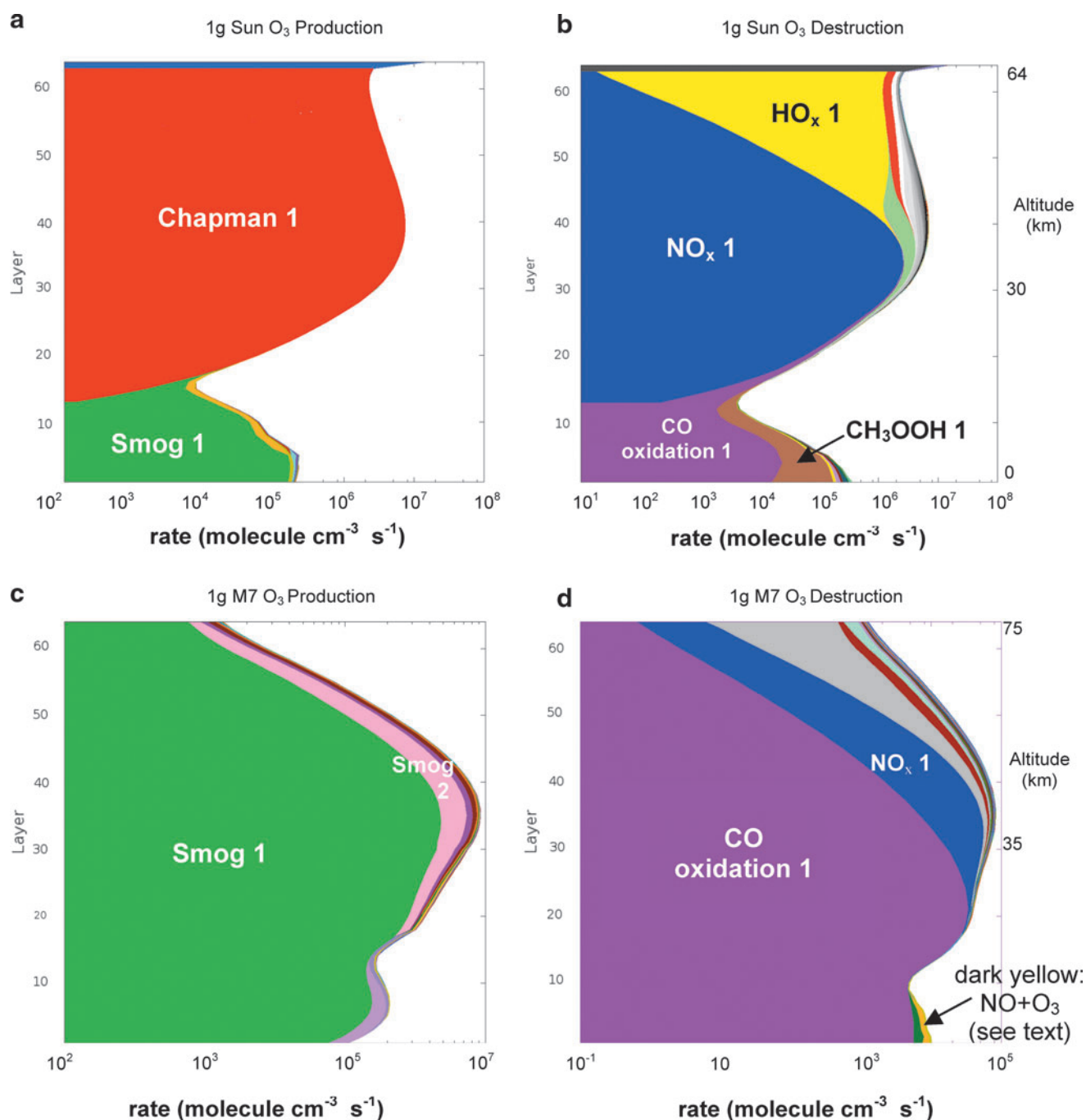


FIG. 6. Pathway analysis results showing cumulative contribution of altitude-dependent O₃ production and loss pathways for the 1g Sun (a, b) and for the 1g M7 scenarios (c, d) plotted in the vertical and shown in molecules cm⁻³ s⁻¹. Black and white labels on the figure correspond to the names of the individual cycles as shown in Appendix A1. Logarithmic x axis tick labels correspond to factors of $\times 2$, $\times 5$, and $\times 8$, respectively. Note that the model vertical grid is variable depending on, *e.g.*, greenhouse gas heating, which leads to an expansion in the vertical for cooler effective stellar temperatures. Color images available online at www.liebertonline.com/ast

high O₃ concentrations, (ii) the reaction $\text{HO}_2 + \text{O}_3 \rightarrow \text{OH} + 2\text{O}_2$ favors the “CO-oxidation 1” pathway. These two effects together favor large smog rates for the M5 and M7 scenarios. In summary, total vertically integrated O₃ production and loss rates for the 1g Sun (1.9×10^{13} molecules cm⁻² s⁻¹) are 68 times larger than for the 1g M7 case (2.8×10^{11} molecules cm⁻² s⁻¹), which illustrates the change in the dominance from the rather fast Chapman chemistry to the slower smog mechanism.

3.5.7. N₂O column-integrated pathways. The main result of PAP is that loss pathways from the N₂O “viewpoint” are noncatalytic for all scenarios. In other words, loss occurs mainly directly via photolysis, which can be calculated from the photolysis rate without performing a PAP analysis for N₂O. We therefore only show (Appendix A1.2) one scenario as an illustration, that is, the Sun scenario, which confirms results measured for Earth, that is, $\sim 95\%$ loss via photolysis

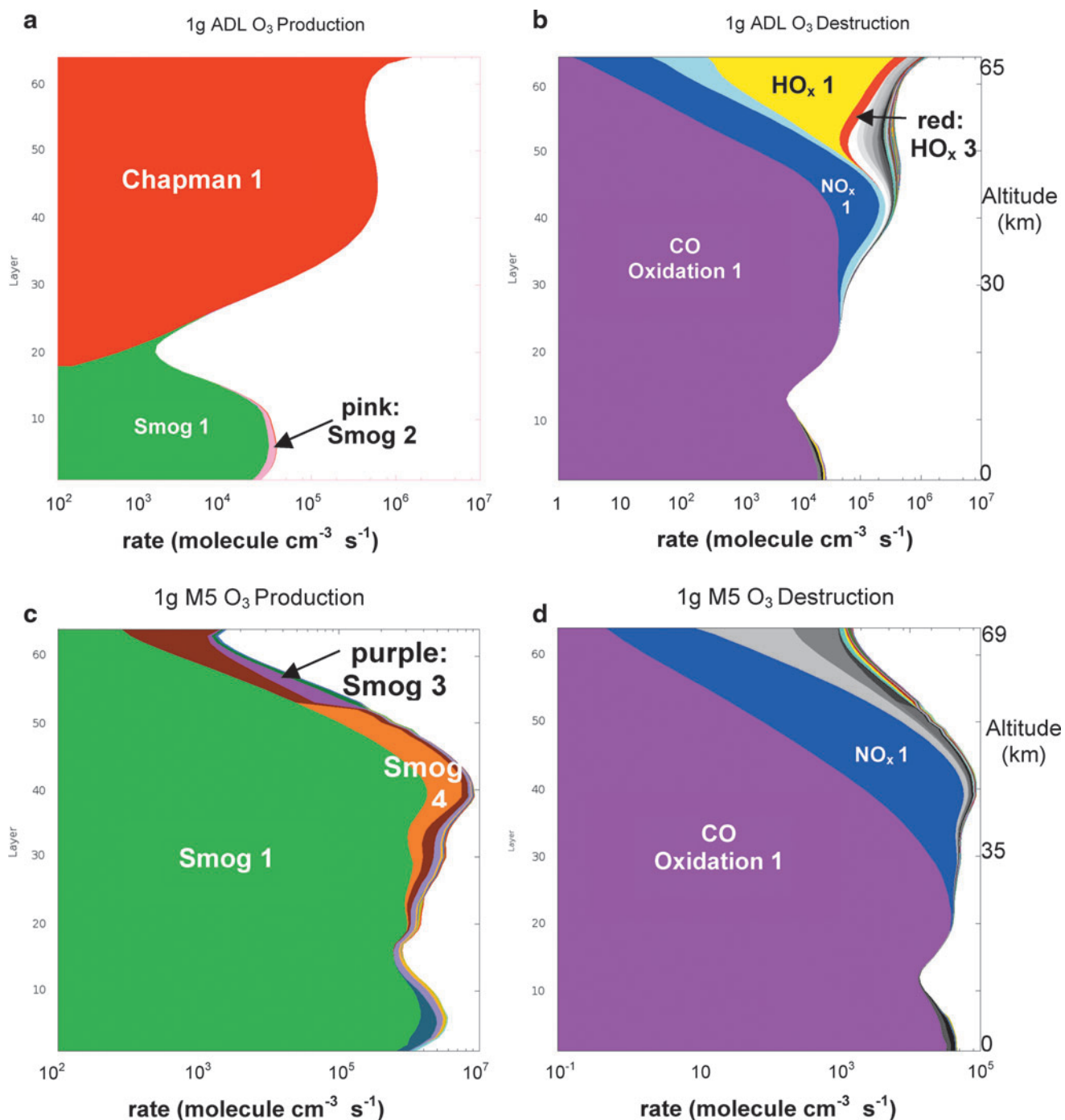


FIG. 7. As for Fig. 6 but for the 1g ADL (a, b) and for the 1g M5 scenarios (c, d). Color images available online at www.liebertonline.com/ast

(i.e., the sum of the four cycles involving N₂O photolysis in Appendix A1.2), and ~5% loss via catalytic reaction with O(¹D) is similar to observed values quoted for Earth [e.g., 90–95% photolytic loss, 5–10% via reaction with O(¹D)], IPCC Third Assessment Report by Houghton *et al.* (2001), see discussion for Table 4.4]. PAP finds no formation pathways of N₂O via inorganic reactions, as expected since these are insignificant compared with surface biogenic input. For the M dwarf scenarios, photolysis similarly remained the main removal mechanism, and the overall column integrated rate of

removal decreased by about a factor of two for the M7 compared with the Sun case since the cooler stars emit less UV.

3.5.8. CH₄ column-integrated pathways. Appendix A1.3 shows the PAP output for CH₄. Results suggest a large number of complex removal pathways that oxidize CH₄. PAP found no *in situ* production pathways, since there are no inorganic reactions in our model that produce CH₄ in the atmosphere. The net removal can involve complete oxidation of CH₄ to its stable combustion products, H₂O and CO₂ (as in

the “Oxidation 2O₂-a” pathway for the 1g Sun scenario), but can also involve only partial oxidation, for example, to intermediate organic species such as formaldehyde (HCHO), for example, as in the “Oxidation O₂” pathway (1g M0). Clearly, more complete oxidation is favored in oxidizing environments, for example, damp atmospheres with strong UV where OH is abundant.

The choice of oxidant in the net reaction will depend on the central star’s particular UVB radiation output and its ability to release, for example, HO_x, O_x, or NO_x from their reservoirs in the planetary atmosphere. Importantly for O₃ photochemistry, there are CH₄ cycles in which O₃ itself is the oxidant in the net reaction (see, *e.g.*, net reaction for several cycles from the 3g Sun case). This is an example where CH₄ oxidation does not lead to the more familiar O₃ (smog) production but to the reverse effect where O₃ is consumed. Many of the CH₄ pathways are NO_x catalyzed, as on Earth, although this is not the case for all scenarios [*e.g.*, pathway “CH₃OOH-d” (3g M5) does not include NO_x].

3.6. Altitude-dependent PAP results

In this section we will present PAP results from the same scenarios as the previous section. However, here we will discuss the contribution of the PAP cycles as profiles varying in the vertical.

3.6.1. Vertical changes in ozone (O₃) production and loss cycles. Figure 6 shows the altitude-dependent PAP results, comparing production and loss pathways for the Earth case (Fig. 6a, 6b) with the M7 case (Fig. 6c, 6d). Similarly, Fig. 7a, 7b compare ADL (1g) with M5 (1g) (Fig. 7c, 7d). In Figs. 6 and 7, the logarithmic *x* axis shows the rate of change of O₃ associated with a particular cycle found by PAP, in molecules cm⁻³ s⁻¹. Note that the logarithmic *x* axis where results are plotted cumulatively (meaning to estimate the contribution of a pathway at a particular height one must subtract its left-hand *x* axis boundary from its right-hand *x* axis boundary) in Figs. 6 and 7 means that the pathways shown on the right-hand side of the figure can make up a strong overall contribution to the net rate of change despite having only a thin section (relatively small area).

For the Earth results (Fig. 6a, 6b), the O₃ production and loss rates output by PAP compare well with middle atmosphere O₃ budgets derived for Earth; see for example the work of Jucks *et al.* (1996), their Fig. 4. The Earth results (Fig. 6a) in the top model layer show an uppermost region of O₃ production (thin, blue stripe), which arose due to the single reaction O₂+O(³P)+M→O₃+M. This is linked with the model’s upper boundary condition, where a downward flux of CO and O(³P) is imposed. This is done to parameterize the effects of CO₂ photolysis [forming CO and O(³P)], which takes place above the model’s lid, for example, above the mid mesosphere. The resulting enhanced O(³P) in the uppermost model layer favors the direct O₃ formation pathway found by PAP. The enhanced O₃ source was balanced by an increase in the photolysis rate of O₃; therefore the abundance decreased smoothly with altitude as expected. The effect of varying the upper boundary will be the subject of future work. NO_x loss cycles dominate (>60%) the Earth’s lower stratosphere; HO_x cycles are more important in the upper stratosphere. For the 3g case (3g Sun), the O₃ production

pathways are similar to those of Earth, but HO_x destruction is stronger (~70%) in the lower stratosphere, which is consistent with more UV penetration (releasing HO_x from its reservoirs) for the thinner (3g) atmospheric column compared with the 1g case. The enhanced tropospheric HO_x, which also stimulated the “CO-oxidation 1” cycle, accounted for 30–50% of tropospheric O₃ loss.

For the warm M dwarf star scenarios (*e.g.*, 1g M0), here, like the control (1g Sun), “Smog 1” dominates 50–60% of the O₃ production in the troposphere (with 10–20% arising from CH₄ smog cycles). The influence of the smog mechanism extends to high altitudes (up to about 20 km) compared with the Earth control (which extends up to about 16 km). “Chapman 1” (Appendix A1.1) dominated the stratosphere. O₃ loss was dominated by the “CO-oxidation 1” pathway (60–80%) in the troposphere, NO_x loss pathways in the mid stratosphere, and HO_x loss pathways in the upper stratosphere. For the 3g case (3g M0), the “Smog 1” pathway contributes ~70% of O₃ production in the troposphere with the ~10–15% remainder in the troposphere coming from CH₄ smog pathways. “Chapman 1” is dominant in the stratosphere, and “Chapman 2” is dominant in the uppermost layers (see discussion above for Earth run 1). O₃ loss, like the 1g case, was dominated by the “CO-oxidation 1” pathway in the troposphere (~90%) with different HO_x cycles important for loss in the upper levels.

In Fig. 7, ADL O₃ photochemistry production (Fig. 7a) is rather similar, for example, to the Earth control (1g Sun) case (Fig. 6a), in that Chapman production dominates the stratosphere and smog the troposphere. However, for the 1g M5 run, results are very different from what occurs on Earth, since O₃ production is now dominated by the smog mechanism through much of the atmosphere. For ADL, O₃ production occurred mostly via “Smog 1” (70–80%) in the troposphere, with various CH₄ smog pathways making up between 10% and 20% in this region. “Chapman 1” dominated the stratosphere. O₃ loss was again dominated by “CO-oxidation 1” in the troposphere (70–90%) with a variety of HO_x cycles important for loss in the upper levels. Intense Lyman-alpha radiation favored some enhancement of H₂O photolysis (hence more O₃ loss via HO_x) in the 1g ADL scenario compared to, for example, the Earth control (run 1), but the effect was quickly damped (in the uppermost ~2 model layers), and the overall change in O₃ was small. For the corresponding 3g case (3g ADL), O₃ production pathways did not change greatly with altitude compared with the 1g case. O₃ loss pathways were also rather similar to the 1g ADL case, with the “CO-oxidation 1” pathway for 3g ADL dominating the lower atmosphere.

The cooler stars (M5, M7) show significant changes in the O₃ photochemistry compared with the other M dwarf scenarios. The rather weak UV radiation of these cooler stars means that Chapman chemistry (requiring UV to break the strong O₂ molecule) is now only significant (up to ~50% O₃ production) (1g M5) in the uppermost (>60 km) altitudes. The “CO-smog 1” pathway, however, is now significant over all altitudes, accounting for 60% of O₃ production in the troposphere and about 30% in the upper atmosphere. A variety of CH₄ smog pathways make up most of the remaining O₃ production (1g M5). For O₃ loss, the “CO-oxidation 1” pathway is again significant (50–70%) in the lower half of the model domain, whereas a variety of NO_x cycles

are important in the upper regions. For the coolest star considered (1g M7), the O_3 abundance is determined by mainly CO and CH_4 oxidation. First, “classical” smog production—with OH as the oxidant (mainly “CO-smog 1” and various CH_4 oxidation pathways)—produces O_3 ; but, on the other hand, O_3 in the M7 scenario can also act as an oxidant in pathways that oxidize, for example, CH_4 and CO.

The M7 case (Fig. 6c, 6d) shows that the CO smog mechanism dominates the O_3 production, whereas the CO oxidation cycle and the classical NO_x cycle dominate the O_3 loss. Near the surface, some direct removal of O_3 occurred via the reaction $NO + O_3 \rightarrow O_2 + NO_2$ (Fig. 6d). On Earth, more NO_x usually leads to more O_3 production via the smog mechanism; the direct removal reaction is, however, sometimes important at high NO_x abundances, for example, in city centers. In our M7 scenario, which does not have industrial NO_x emissions, an important source of lower atmosphere NO_x is from lightning. For the cool M dwarf 3g case (3g M5, not shown), the “CO-smog 1” and “Chapman 1” pathways make almost equal contributions to the O_3 production budget in the middle atmosphere. “Chapman 1” contributes up to $\sim 80\%$ of local production in the upper levels (where UV is abundant), whereas the smog mechanism contributes up to $\sim 70\%$ in the lower layers. The smog contribution has a minimum of $\sim 20\%$ local production near the cold trap, which is consistent with low temperatures and a rather low OH abundance. For the O_3 loss pathways, results suggest an increase in complex CO and CH_4 smog pathways that consume O_3 .

3.6.2. N_2O . For all scenarios, noncatalytic photolytic removal ($>90\%$) is the main loss mechanism in the stratosphere. Catalytic removal involving reaction with $O(^1D)$ makes up the remainder (occurring mostly in the mid to upper stratosphere) of the N_2O loss.

3.6.3. CH_4 . Results suggest that a large number of loss pathways occur near the cold trap. For example, at 16 km (1g Sun), the CH_4 pathways found by PAP with the value of f_{\min} chosen in this study could account for only about 20% of the total CH_4 change calculated in the column model. Low OH abundances and cold temperatures in this region are consistent with rather slow oxidation and a resulting complex mix of only weakly oxidized organic species with individual pathway contributions lying below the PAP threshold criteria chosen for the present study but whose net effect is important. For this study, the PAP detection threshold was set to $f_{\min} = 10^{-8}$ ppbv/s. OH-initiated oxidation of CH_4 is more favored on the lower layers but with relatively more $O(^1D)$ -initiated oxidation on the upper levels, where this species is more abundant. A test run (not shown) where the f_{\min} value is decreased to 10^{-9} ppbv/s was found to address the above problem, that is, PAP was then able to account, for example, 3 times more CH_4 net change (for the Earth run), though with a notable increase in the overall number of pathways, each with small contributions to net the overall chemical change, beyond the scope of our work.

3.7. Comparison with previous studies

Compared with the results of Segura *et al.* (2005), our results are similar for N_2O and CH_4 within 10–20% for the

inactive (*e.g.*, M4) and active (ADL) cases. For O_3 , our atmospheric column amounts are $\sim 40\%$ thicker (270 DU) compared with the Segura *et al.* (2005) (164 DU) value for the ADL case. This results from changes in our photochemical scheme, including, for example, the parameterization of the lower boundary flux of H_2 , as discussed in Paper 1. Also, our stellar insolation corresponds to $1366 W m^{-2}$ at the TOA, whereas Segura *et al.* (2005) scaled their incoming spectrum to obtain a surface temperature of 288 K.

4. Spectral Detectability of Biomarkers

4.1. O_3

Paper 1 shows that the detection of O_3 is challenging especially for M7. To better understand O_3 detectability, improved stellar spectra for the cooler stars in the (E)UV are desirable especially in the UVB and UVC, where O_3 responds sensitively. M7 stars are statistically older and burn more slowly compared with lower spectral class stars, which means more developed convection zones and possibly larger differences in UV between flaring and quiet states for M7 than considered in our work (see Reiniers *et al.*, 2012).

4.2. N_2O

Clearly, the most favorable (planet/star) contrast ratios are associated with cool stars such as M7. However, Paper 1 shows that some spectral absorption features can be weakened, partly due to the large CH_4 abundance, which warms the stratosphere. The N_2O spectral features were weak for the scenarios analyzed.

5. Conclusions

- The potential complex-life biosignature O_3 has a very different photochemistry for planets orbiting in the HZ of cool M dwarf stars compared to that of Earth since the key mechanism switches from Chapman production to slower, smog production. Expected responses of O_3 produced by the smog cycle (which could be favored by increases in HO_x and NO_x , *e.g.*, by cosmic rays) could be very different than Chapman-produced O_3 (where HO_x and NO_x catalytically destroy O_3). This is important to consider when predicting and interpreting O_3 spectral features.
- The simple microbial-life biosignature N_2O increases for the cooler stars, mostly related to weaker photolytic loss of N_2O via weaker UVB in the middle atmosphere, as found too by earlier studies. In some cases, however, variations in transport become important. The amount of N_2O in the middle atmosphere depends on the UV and on the rate at which this species can be transported upward from the troposphere into the stratosphere where it is photolyzed.
- The greenhouse gas CH_4 responses and its removal pathways become complex especially for the cooler stars. CH_4 abundances generally increase for the cooler stars, a result also found in earlier studies, due to a lowering in OH, its main sink, which is associated mainly with a weakening in the main OH source reaction that requires UVB.
- The potential vegetation biosignature CH_3Cl is enhanced in abundance by more than three orders of

magnitude compared with the Earth run especially for cool M star scenarios associated with low OH since reaction with this species is the main sink (see also CH₄ above). Like earlier studies, our results suggest that its spectral features are nevertheless very weak.

- Comparison of the 1g and 3g scenarios suggests that it is important to include interactive photochemistry when calculating biosignatures and greenhouse gas abundances. Reducing the mass of the atmosphere by, for example, a factor of 3 does not always lead to a reduction in, for example, biosignatures and greenhouse gases by a factor of 3, due to interactive climate-photochemical effects.

Appendix A1

“**Found_PAP**” denotes the CIR (in molecules cm⁻² s⁻¹) of change shown for production and loss for all atmospheric pathways **found** by PAP. “**Shown_PAP**” denotes the CIR only for the pathways **shown** in this appendix. Shown are either the five dominant pathways or the first pathways which together account for >90% of Found_PAP, whichever criterion is fulfilled first. “**Total_chem**” denotes the CIR as calculated in the **chemistry** scheme of the atmospheric column model. **Percent** values for a particular cycle show its individual rate as a percentage of Found_PAP.

A1.1. Ozone pathways

TABLE A1.1A. 1g SUN OZONE PRODUCTION

Chapman 1 (90.5%)	Chapman 2 (8.3%)	Smog 1 (0.8%)
$O_2 + hv \rightarrow O(^3P) + O(^3P)$	$O(^3P) + O_2 + M \rightarrow O_3 + M$	$CO + OH \rightarrow CO_2 + H$
$2(O(^3P) + O_2 + M \rightarrow O_3 + M)$	net: $O(^3P) + O_2 + M \rightarrow O_3 + M$	$H + O_2 + M \rightarrow HO_2 + M$
net: $3O_2 \rightarrow 2O_3$		$NO + HO_2 \rightarrow NO_2 + OH$
		$NO_2 + hv \rightarrow NO + O(^3P)$
		$O(^3P) + O_2 + M \rightarrow O_3 + M$
		net: $CO + 2O_2 \rightarrow O_3 + CO_2$

Found_PAP = 1.88×10^{13} , Shown_PAP = 1.87×10^{13} , Total_chem = 1.88×10^{13} .

TABLE A1.1B. 1g SUN OZONE LOSS

NO _x 1 (17.6%)	HO _x 1 (15.6%)	NO _x 2 (12.3%)	O _x 1 (6.9%)	HO _x 2 (6.3%)
$O_3 + hv \rightarrow O_2 + O(^3P)$	$2(O_3 + hv \rightarrow O_2 + O(^1D))$	$O_3 + hv \rightarrow O_2 + O(^1D)$	$O_3 + hv \rightarrow O_2 + O(^1D)$	$2(O_3 + hv \rightarrow O_2 + O(^1D))$
$NO_2 + O(^3P) \rightarrow NO + O_2$	$2(O(^1D) + N_2 \rightarrow O(^3P) + N_2)$	$O(^1D) + N_2 \rightarrow O(^3P) + N_2$	$O(^1D) + N_2 \rightarrow O(^3P) + N_2$	$2(O(^1D) + O_2 \rightarrow O(^3P) + O_2)$
$NO + O_3 \rightarrow NO_2 + O_2$	$HO_2 + O(^3P) \rightarrow OH + O_2$	$NO_2 + O(^3P) \rightarrow NO + O_2$	$O(^3P) + O_3 \rightarrow O_2 + O_2$	$HO_2 + O(^3P) \rightarrow OH + O_2$
net: $2O_3 \rightarrow 3O_2$	$OH + O(^3P) \rightarrow H + O_2$	$NO + O_3 \rightarrow NO_2 + O_2$	$2O_3 \rightarrow 3O_2$	$OH + O(^3P) \rightarrow H + O_2$
	$H + O_2 + M \rightarrow HO_2 + M$	$2O_3 \rightarrow 3O_2$		$H + O_2 + M \rightarrow HO_2 + M$
	$2O_3 \rightarrow 3O_2$			$2O_3 \rightarrow 3O_2$

Found_PAP = 1.81×10^{13} , Shown_PAP = 1.06×10^{13} , Total_chem = 1.88×10^{13} .

TABLE A1.1C. 3g SUN OZONE PRODUCTION

Chapman 1 (99.3%)	Smog 1 (0.3%)
-------------------	---------------

Found_PAP = 1.28×10^{13} , Shown_PAP = 1.27×10^{13} , Total_chem = 1.28×10^{13} .

TABLE A1.1D. 3g SUN OZONE LOSS

HO _x 1 (17.7%)	O _x 1 (9.5%)	NO _x 2 (8.3%)	O _x 2 (7.6%)	NO _x 1 (7.3%)
			$O_3 + hv \rightarrow O_2 + O(^3P)$	
			$O(^3P) + O_3 \rightarrow O_2 + O_2$	
			$2O_3 \rightarrow 3O_2$	

Found_PAP = 1.20×10^{13} , Shown_PAP = 6.06×10^{12} , Total_chem = 1.26×10^{13} .

TABLE A1.1E. 1g M0 OZONE PRODUCTION

Chapman 1 (89.2%)	Smog 1 (7.9%)	Smog 2 (1.2%)
		$\text{CH}_4 + \text{OH} \rightarrow \text{CH}_3 + \text{H}_2\text{O}$ $\text{CH}_3 + \text{O}_2 + \text{M} \rightarrow \text{CH}_3\text{O}_2 + \text{M}$ $\text{CH}_3\text{O}_2 + \text{NO} \rightarrow \text{H}_3\text{CO} + \text{NO}_2$ $\text{H}_3\text{CO} + \text{O}_2 \rightarrow \text{H}_2\text{CO} + \text{HO}_2$ $\text{H}_2\text{CO} + h\nu \rightarrow \text{H}_2 + \text{CO}$ $\text{NO} + \text{HO}_2 \rightarrow \text{NO}_2 + \text{OH}$ $2(\text{NO}_2 + h\nu \rightarrow \text{NO} + \text{O}({}^3\text{P}))$ $2(\text{O}({}^3\text{P}) + \text{O}_2 + \text{M} \rightarrow \text{O}_3 + \text{M})$ net: $\text{CH}_4 + 4\text{O}_2 \rightarrow 2\text{O}_3 + \text{H}_2\text{O} + \text{H}_2 + \text{CO}$

Found_PAP = 1.65×10^{12} , Shown_PAP = 1.63×10^{12} , Total_chem = 1.70×10^{12} .

TABLE A1.1F. 1g M0 OZONE LOSS

NO _x 1 (25.4%)	HO _x 1 (11.1%)	HO _x 3 (7.5%)	CO-oxidation 1 (7.4%)	NO _x 1 (7.1%)
		$2(\text{O}_3 + h\nu \rightarrow \text{O}_2 + \text{O}({}^3\text{P}))$ $\text{HO}_2 + \text{O}({}^3\text{P}) \rightarrow \text{OH} + \text{O}_2$ $\text{OH} + \text{O}({}^3\text{P}) \rightarrow \text{H} + \text{O}_2$ $\text{H} + \text{O}_2 + \text{M} \rightarrow \text{HO}_2 + \text{M}$ net: $2\text{O}_3 \rightarrow 3\text{O}_2$ (7.5%)	$\text{HO}_2 + \text{O}_3 \rightarrow \text{OH} + \text{O}_2 + \text{O}_2$ $\text{CO} + \text{OH} \rightarrow \text{CO}_2 + \text{H}$ $\text{H} + \text{O}_2 + \text{M} \rightarrow \text{HO}_2 + \text{M}$ net: $\text{O}_3 + \text{CO} \rightarrow \text{O}_2 + \text{CO}_2$	

Found_PAP = 1.52×10^{12} , Shown_PAP = 8.92×10^{11} , Total_chem = 1.64×10^{12} .

TABLE A1.1G. 3g M0 OZONE PRODUCTION

Chapman 1 (96.7%)	Smog 1 (2.6%)	Chapman 2 (0.3%)
Found_PAP = 1.31×10^{12} , Shown_PAP = 1.30×10^{12} , Total_chem = 1.32×10^{12} .		

TABLE A1.1H. 3g M0 OZONE LOSS

CO-oxidation 1 (17.6%)	HO _x 1 (12.%)	NO _x 1 (10.3%)	HO _x 3 (8.1%)	HO _x 4 (5.8%)
				$\text{HO}_2 + \text{O}_3 \rightarrow \text{OH} + \text{O}_2 + \text{O}_2$ $\text{OH} + \text{O}_3 \rightarrow \text{HO}_2 + \text{O}_2$ net: $2\text{O}_3 \rightarrow 3\text{O}_2$

Total = Found_PAP = 9.75×10^{11} , Shown_PAP = 5.27×10^{11} , Total_chem = 1.20×10^{12} .

TABLE A1.1I. 1g ADL OZONE PRODUCTION

Chapman 1 (97.2%)	Smog 1 (2.3%)	Smog 3 (0.3%)
		$\text{CH}_4 + \text{OH} \rightarrow \text{CH}_3 + \text{H}_2\text{O}$ $\text{CH}_3 + \text{O}_2 + \text{M} \rightarrow \text{CH}_3\text{O}_2 + \text{M}$ $\text{CH}_3\text{O}_2 + \text{NO} \rightarrow \text{H}_3\text{CO} + \text{NO}_2$ $\text{H}_3\text{CO} + \text{O}_2 \rightarrow \text{H}_2\text{CO} + \text{HO}_2$ $2(\text{NO}_2 + h\nu \rightarrow \text{NO} + \text{O}({}^3\text{P}))$ $\text{NO} + \text{HO}_2 \rightarrow \text{NO}_2 + \text{OH}$ $2(\text{O}({}^3\text{P}) + \text{O}_2 + \text{M} \rightarrow \text{O}_3 + \text{M})$ net: $\text{CH}_4 + 4\text{O}_2 \rightarrow 2\text{O}_3 + \text{H}_2\text{CO} + \text{H}_2\text{O}$

Found_PAP = 1.72×10^{12} , Shown_PAP = 1.71×10^{12} , Total_chem = 1.72×10^{12} .

TABLE A1.1j. 1g ADL OZONE LOSS

NO_x 1 (12.6%)	HO_x 1 (12.3%)	CO-oxidation 1 (9.0%)	HO_x 3 (7.5%)	O_x 2 (5.4%)
---------------------------------	---------------------------------	------------------------------	--------------------------------	-------------------------------

Found_PAP = 1.43×10^{12} , Shown_PAP = 6.71×10^{11} , Total_chem = 1.69×10^{12} .

TABLE A1.1k. 3g ADL OZONE PRODUCTION

Chapman 1 (99.5%)	Smog 1 (0.4%)
--------------------------	----------------------

Found_PAP = 1.56×10^{12} , Shown_PAP = 1.56×10^{12} , Total_chem = 1.56×10^{12} .

TABLE A1.1l. 3g ADL OZONE LOSS

HO_x 1 (12.4%)	CO-oxidation 1 (10.4%)	HO_x 3 (7.6%)	HO_x 5 (6.2%)	CO-oxidation 2 (5.7%)
			$O_3 + hv \rightarrow O_2 + O(^1D)$	$O_3 + hv \rightarrow O_2 + O(^1D)$
			$O(^1D) + N_2 \rightarrow O(^3P) + N_2$	$O(^1D) + N_2 \rightarrow O(^3P) + N_2$
			$OH + O(^3P) \rightarrow H + O_2$	$HO_2 + O(^3P) \rightarrow OH + O_2$
			<u>$H + O_3 \rightarrow OH + O_2$</u>	$CO + OH \rightarrow CO_2 + H$
			net: $2O_3 \rightarrow 3O_2$	<u>$H + O_2 + M \rightarrow HO_2 + M$</u>
				net: $O_3 + CO \rightarrow O_2 + CO_2$

Found_PAP = 1.13×10^{12} , Shown_PAP = 4.78×10^{11} , Total_chem = 1.34×10^{12} .

TABLE A1.1m. 1g M5 OZONE PRODUCTION

Smog 1 (57.8%)	Smog 4 (17.3%)	Chapman 1 (7.5%)	Smog 2 (6.8%)	Smog 3 (4.1%)
	$CH_4 + OH \rightarrow CH_3 + H_2O$			
	$CH_3 + O_2 + M \rightarrow CH_3O_2 + M$			
	$CH_3O_2 + NO \rightarrow H_3CO + NO_2$			
	$H_3CO + O_2 \rightarrow H_2CO + HO_2$			
	$H_2CO + OH \rightarrow H_2O + HCO$			
	$HCO + O_2 \rightarrow HO_2 + CO$			
	$2(NO + HO_2 \rightarrow NO_2 + OH)$			
	$3(NO_2 + hv \rightarrow NO + O(^3P))$			
	<u>$3(O(^3P) + O_2 + M \rightarrow O_3 + M)$</u>			
	$CH_4 + 6O_2 \rightarrow 3O_3 + 2H_2O + CO$			

Found_PAP = 2.92×10^{11} , Shown_PAP = 2.72×10^{11} , Total_chem = 3.24×10^{11} .

TABLE A1.1n. 1g M5 OZONE LOSS

CO-oxidation 1 (36.8%)	NO_x 1 (35.2%)	Smog 5 (6.4%)	Smog 6 (3.8%)	NO_x 2 (3.0%)
		$O_3 + hv \rightarrow O_2 + O(^3P)$	$3(O_3 + hv \rightarrow O_2 + O(^3P))$	
		$NO_2 + O(^3P) \rightarrow NO + O_2$	$3(NO_2 + O(^3P) \rightarrow NO + O_2)$	
		$NO + HO_2 \rightarrow NO_2 + OH$	$2(NO + HO_2 \rightarrow NO_2 + OH)$	
		$CO + OH \rightarrow CO_2 + H$	$CH_4 + OH \rightarrow CH_3 + H_2O$	
		<u>$H + O_2 + M \rightarrow HO_2 + M$</u>	$CH_3 + O_2 + M \rightarrow CH_3O_2 + M$	
		$O_3 + CO \rightarrow O_2 + CO_2$	$CH_3O_2 + NO \rightarrow H_3CO + NO_2$	
			$H_3CO + O_2 \rightarrow H_2CO + HO_2$	
			$H_2CO + OH \rightarrow H_2O + HCO$	
			<u>$HCO + O_2 \rightarrow HO_2 + CO$</u>	
			$3O_3 + CH_4 \rightarrow 2H_2O + CO + 3O_2$	

Found_PAP = 2.57×10^{11} , Shown_PAP = 2.19×10^{11} , Total_chem = 2.91×10^{11} .

TABLE A1.1o. 3g M5 OZONE PRODUCTION

Chapman 1 (47.8%)	Smog 1 (47.6%)	Chapman 2 (2.4%)
--------------------------	-----------------------	-------------------------

Found_PAP = 1.35×10^{11} , Shown_PAP = 1.32×10^{11} , Total_chem = 1.42×10^{11} .

TABLE A1.1P. 3g M5 OZONE LOSS

CH ₃ OOH 1 (46.8%)	CH ₄ -O ₃ oxidation (6.2%)	CO-oxidation 3 (5.1%)	H ₂ O ₂ cycle (4.6%)
O ₃ + hv → O ₂ + O(¹ D)	O ₃ + hv → O ₂ + O(¹ D)	O ₃ + hv → O ₂ + O(³ P)	O ₃ + hv → O ₂ + O(¹ D)
CH ₄ + O(¹ D) → CH ₃ + OH	<u>CH₄ + O(¹D) → H₂CO + H₂</u>	HO ₂ + O(³ P) → OH + O ₂	H ₂ O + O(¹ D) → OH + OH
CH ₃ + O ₂ + M → CH ₃ O ₂ + M	net: O ₃ + CH ₄ → H ₂ CO + H ₂ + O ₂	CO + OH → CO ₂ + H	2(CO + OH → CO ₂ + H)
CO + OH → CO ₂ + H		<u>H + O₂ + M → HO₂ + M</u>	2(H + O ₂ + M → HO ₂ + M)
H + O ₂ + M → HO ₂ + M		net: O ₃ + CO → O ₂ + CO ₂	<u>HO₂ + HO₂ → H₂O₂ + O₂</u>
<u>CH₃O₂ + HO₂ → CH₃OOH + O₂</u>			net: O ₃ + H ₂ O + 2CO → H ₂ O ₂ + 2CO ₂
net: O ₃ + CH ₄ + CO → CH ₃ OOH + CO ₂			

Found_PAP = 1.19 × 10¹¹, Shown_PAP = 1.08 × 10¹¹, Total_chem = 1.28 × 10¹¹.

TABLE A1.1Q. 1g M7 OZONE PRODUCTION

Smog 1 (58.8%)	Smog 3 (22.9%)	CH ₃ OOH 2 smog cycle (6.0%)	HCHO cycle (4.9%)
		2(NO ₂ + hv → NO + O(³ P))	NO ₂ + hv → NO + O(³ P)
		2(O(³ P) + O ₂ + M → O ₃ + M)	NO + HO ₂ → NO ₂ + OH
		NO + HO ₂ → NO ₂ + OH	H ₂ CO + OH → H ₂ O + HCO
		CH ₃ OOH + OH → CH ₃ O ₂ + H ₂ O	HCO + O ₂ → HO ₂ + CO
		CH ₃ O ₂ + NO → H ₃ CO + NO ₂	<u>O(³P) + O₂ + M → O₃ + M</u>
		<u>H₃CO + O₂ → H₂CO + HO₂</u>	net: H ₂ CO + 2O ₂ → O ₃ + H ₂ O + CO
		net: CH ₃ OOH + 3O ₂ → 2O ₃ + H ₂ CO + H ₂ O	

Found_PAP = 2.79 × 10¹¹, Shown_PAP = 2.59 × 10¹¹, Total_chem = 2.92 × 10¹¹.

TABLE A1.1R. 1g M7 OZONE LOSS

NO _x 1 (33.1%)	CO-oxidation 1 (28.3%)	Smog 5 (11.5%)	Smog 7 (6.4%)	NO _x 3 (3.3%)
			2(O ₃ + hv → O ₂ + O(³ P))	2(NO + O ₃ → NO ₂ + O ₂)
			2(NO ₂ + O(³ P) → NO + O ₂)	NO ₂ + hv → NO + O(³ P)
			NO + HO ₂ → NO ₂ + OH	<u>NO₂ + O(³P) → NO + O₂</u>
			CH ₄ + OH → CH ₃ + H ₂ O	net: 2O ₃ → 3O ₂
			CH ₃ + O ₂ + M → CH ₃ O ₂ + M	
			CH ₃ O ₂ + NO → H ₃ CO + NO ₂	
			<u>H₃CO + O₂ → H₂CO + HO₂</u>	
			net: 2O ₃ + CH ₄ → H ₂ CO + H ₂ O + 2O ₂	

Found_PAP = 2.43 × 10¹¹, Shown_PAP = 2.01 × 10¹¹, Total_chem = 2.74 × 10¹¹.

A1.2. Nitrous oxide pathways (Sun only)

TABLE A1.2A. 1g SUN NITROUS OXIDE LOSS

N ₂ O-NO _x (69.5%)	N ₂ O-O _x (9.6%)	N ₂ -O(¹ D) (5.4%)	N ₂ O-HO _x -1 (3.4%)	N ₂ O-HO _x -2 (3.3%)
2(N ₂ O + hv → N ₂ + O(³ P))	2(N ₂ O + hv → N ₂ + O(³ P))	2(N ₂ O + O(¹ D) → N ₂ + O ₂)	2(N ₂ O + hv → N ₂ + O(³ P))	2(N ₂ O + hv → N ₂ + O(³ P))
O(³ P) + O ₂ + M → O ₃ + M	O(³ P) + O ₂ + M → O ₃ + M	2(O(³ P) + O ₂ + M → O ₃ + M)	2(O(³ P) + O ₂ + M → O ₂ + M)	O(³ P) + O ₂ + M → O ₃ + M
NO ₂ + O(³ P) → NO + O ₂	<u>O(³P) + O₃ → O₂ + O₂</u>	2(O ₃ + hv → O ₂ + O(¹ D))	OH + O ₃ → HO ₂ + O ₂	HO ₂ + O(³ P) → OH + O ₂
<u>NO + O₃ → NO₂ + O₂</u>	net: 2N ₂ O → O ₂ + 2N ₂	<u>O₂ + hv → O(³P) + O(³P)</u>	<u>HO₂ + O₃ → OH + O₂ + O₂</u>	<u>OH + O₃ → HO₂ + O₂</u>
net: 2N ₂ O → O ₂ + 2N ₂		net: 2N ₂ O → O ₂ + 2N ₂	net: 2N ₂ O → O ₂ + 2N ₂	net: 2N ₂ O → O ₂ + 2N ₂

Found_PAP = 9.63 × 10⁸, Shown_PAP = 8.78 × 10⁸, Total_chem = 1.15 × 10⁹.

TABLE A1.3C. 1g M0 METHANE LOSS

Oxidation 3O ₂ -a (24.4%)	Oxidation CH ₃ OOH-b (12.8%)	Oxidation O ₂ (10.4%)	Oxidation 6O ₂ (6.1%)	Oxidation CH ₃ OOH-c (5.7%)
CH ₄ + OH → CH ₃ + H ₂ O	CH ₄ + OH → CH ₃ + H ₂ O	CH ₄ + OH → CH ₃ + H ₂ O		2(CH ₄ + OH → CH ₃ + H ₂ O)
CH ₃ + O ₂ + M → CH ₃ O ₂ + M	CH ₃ + O ₂ + M → CH ₃ O ₂ + M	CH ₃ + O ₂ + M → CH ₃ O ₂ + M		2(CH ₃ + O ₂ + M → CH ₃ O ₂ + M)
CH ₃ O ₂ + HO ₂ → CH ₃ OOH + O ₂	CH ₃ O ₂ + NO → H ₃ CO + NO ₂	CH ₃ O ₂ + NO → H ₃ CO + NO ₂		CH ₃ O ₂ + HO ₂ → CH ₃ OOH + O ₂
H ₂ O + O(¹ D) → OH + OH	H ₃ CO + O ₂ → H ₂ CO + HO ₂	H ₃ CO + O ₂ → H ₂ CO + HO ₂		CH ₃ O ₂ + NO → H ₃ CO + NO ₂
2(H + O ₂ + M → HO ₂ + M)	HO ₂ + O ₃ → OH + O ₂ + O ₂	HO ₂ + O ₃ → OH + O ₂ + O ₂		H ₃ CO + O ₂ → H ₂ CO + HO ₂
NO + HO ₂ → NO ₂ + OH	NO ₂ + hν → NO + O(³ P)	NO ₂ + hν → NO + O(³ P)		NO ₂ + hν → NO + O(³ P)
2(CO + OH → CO ₂ + H)	<u>O(³P) + O₂ + M → O₃ + M</u>	<u>O(³P) + O₂ + M → O₃ + M</u>		O(³ P) + O ₂ + M → O ₃ + M
NO ₂ + hν → NO + O(³ P)	net: CH ₄ + O ₂ → H ₂ CO + H ₂ O	net: CH ₄ + O ₂ → H ₂ CO + H ₂ O		O ₃ + hν → O ₂ + O(¹ D)
O(³ P) + O ₂ + M → O ₃ + M				<u>H₂O + O(¹D) → OH + OH</u>
<u>O₃ + hν → O₂ + O(¹D)</u>				net: 2CH ₄ + 2O ₂ → H ₂ CO + H ₂ O + CH ₃ OOH
net: CH ₄ + 2CO + 2O ₂ → CH ₃ OOH + 2CO ₂				

Found_PAP = 3.25 × 10¹⁰, Shown_PAP = 1.93 × 10¹⁰, Total_chem = 1.24 × 10¹¹.

TABLE A1.3D. 3g M0 METHANE LOSS

Oxidation CH ₃ OOH-a (12.6%)	Oxidation 2O ₂ -b (8.5%)	Oxidation 2O ₂ -c (6.8%)	Oxidation 2O ₂ -d (5.5%)	Oxidation CH ₃ OOH-b (4.7%)
--	--	--	--	---

Found_PAP = 5.67 × 10¹⁰, Shown_PAP = 2.16 × 10¹⁰, Total_chem = 1.24 × 10¹¹.

TABLE A1.3E. 1g ADL METHANE LOSS

Oxidation 2O ₂ -b (30.0%)	Oxidation 2O ₂ -d (14.7%)	Oxidation 2O ₂ -c (7.3%)	Oxidation 2O ₂ -e (6.2%)	Oxidation 2O ₂ -Cl (6.2%)
CH ₄ + OH → CH ₃ + H ₂ O	CH ₄ + OH → CH ₃ + H ₂ O	CH ₄ + OH → CH ₃ + H ₂ O	CH ₄ + OH → CH ₃ + H ₂ O	CH ₄ + Cl → HCl + CH ₃
CH ₃ + O ₂ + M → CH ₃ O ₂ + M	CH ₃ + O ₂ + M → CH ₃ O ₂ + M	CH ₃ + O ₂ + M → CH ₃ O ₂ + M	CH ₃ + O ₂ + M → CH ₃ O ₂ + M	CH ₃ + O ₂ + M → CH ₃ O ₂ + M
CH ₃ O ₂ + NO → H ₃ CO + NO ₂	CH ₃ O ₂ + NO → H ₃ CO + NO ₂	CH ₃ O ₂ + NO → H ₃ CO + NO ₂	CH ₃ O ₂ + OH → H ₃ CO + HO ₂	CH ₃ O ₂ + OH → H ₃ CO + HO ₂
H ₃ CO + O ₂ → H ₂ CO + HO ₂	H ₃ CO + O ₂ → H ₂ CO + HO ₂	H ₃ CO + O ₂ → H ₂ CO + HO ₂	H ₃ CO + O ₂ → H ₂ CO + HO ₂	H ₃ CO + O ₂ → H ₂ CO + HO ₂
NO ₂ + O(³ P) → NO + O ₂	NO ₂ + O(³ P) → NO + O ₂	NO ₂ + O(³ P) → NO + O ₂	H ₂ CO + OH → H ₂ O + HCO	H ₂ CO + OH → H ₂ O + HCO
H ₂ CO + OH → H ₂ O + HCO	H ₂ CO + OH → H ₂ O + HCO	H ₂ CO + OH → H ₂ O + HCO	HCO + O ₂ → HO ₂ + CO	HCO + O ₂ → HO ₂ + CO
HCO + O ₂ → HO ₂ + CO	HCO + O ₂ → HO ₂ + CO	HCO + O ₂ → HO ₂ + CO	3(HO ₂ + O(³ P) → OH + O ₂)	HCl + OH → Cl + H ₂ O
CO + OH → CO ₂ + H	CO + OH → CO ₂ + H	CO + OH → CO ₂ + H	CO + OH → CO ₂ + H	CO + OH → CO ₂ + H
H + O ₂ + M → HO ₂ + M	H + O ₂ + M → HO ₂ + M	H + O ₂ + M → HO ₂ + M	H + O ₃ → OH + O ₂	H + O ₂ + M → HO ₂ + M
3(HO ₂ + O(³ P) → OH + O ₂)	3(HO ₂ + O(³ P) → OH + O ₂)	3(HO ₂ + O(³ P) → OH + O ₂)	O(³ P) + O ₂ + M → O ₃ + M	4(HO ₂ + O(³ P) → OH + O ₂)
<u>2(O₂ + hν → O(³P) + O(³P))</u>				
net: CH ₄ + 2O ₂ → 2H ₂ O + CO ₂	net: CH ₄ + 2O ₂ → 2H ₂ O + CO ₂	net: CH ₄ + 2O ₂ → 2H ₂ O + CO ₂	net: CH ₄ + 2O ₂ → 2H ₂ O + CO ₂	net: CH ₄ + 2O ₂ → 2H ₂ O + CO ₂

Found_PAP = 6.14 × 10¹⁰, Shown_PAP = 3.95 × 10¹⁰, Total_chem = 1.24 × 10¹¹.

TABLE A1.3F. 3g ADL METHANE LOSS

Oxidation 2O ₂ -b (21.9%)	Oxidation 2O ₂ -c (6.3%)	Oxidation 2O ₂ -d (6.3%)	Oxidation 2O ₂ -e (6.2%)	Oxidation 2O ₂ -f (6.1%)
				$\text{CH}_4 + \text{O}({}^1\text{D}) \rightarrow \text{CH}_3 + \text{OH}$ $\text{CH}_3 + \text{O}_2 + \text{M} \rightarrow \text{CH}_3\text{O}_2 + \text{M}$ $\text{CO} + \text{OH} \rightarrow \text{CO}_2 + \text{H}$ $\text{H} + \text{O}_2 + \text{M} \rightarrow \text{HO}_2 + \text{M}$ $\text{CH}_3\text{O}_2 + \text{HO}_2 \rightarrow \text{CH}_3\text{OOH} + \text{O}_2$ $\text{CH}_3\text{OOH} + \text{OH} \rightarrow \text{CH}_3\text{O}_2 + \text{H}_2\text{O}$ $\text{CH}_3\text{O}_2 + \text{OH} \rightarrow \text{H}_3\text{CO} + \text{HO}_2$ $\text{H}_3\text{CO} + \text{O}_2 \rightarrow \text{H}_2\text{CO} + \text{HO}_2$ $\text{H}_2\text{CO} + \text{OH} \rightarrow \text{H}_2\text{O} + \text{HCO}$ $\text{HCO} + \text{O}_2 \rightarrow \text{HO}_2 + \text{CO}$ $3(\text{HO}_2 + \text{O}({}^3\text{P}) \rightarrow \text{OH} + \text{O}_2)$ $\text{O}({}^3\text{P}) + \text{O}_2 + \text{M} \rightarrow \text{O}_3 + \text{M}$ $\text{O}_3 + h\nu \rightarrow \text{O}_2 + \text{O}({}^1\text{D})$ $\underline{2(\text{O}_2 + h\nu \rightarrow \text{O}({}^3\text{P}) + \text{O}({}^3\text{P}))}$ net: $\text{CH}_4 + 2\text{O}_2 \rightarrow 2\text{H}_2\text{O} + \text{CO}_2$

Found_PAP = 7.06×10^{10} , Shown_PAP = 3.31×10^{10} , Total_chem = 1.24×10^{11} .

TABLE A1.3G. 1g M5 METHANE LOSS

Oxidation 2O ₂ (35.5%)	Oxidation 3O ₂ -a (12.7%)	Oxidation O ₂ (11.4%)	Oxidation 3O ₂ -b (6.7%)	Oxidation 2O ₂ -g (5.3%)
$\text{CH}_4 + \text{OH} \rightarrow \text{CH}_3 + \text{H}_2\text{O}$ $\text{CH}_3 + \text{O}_2 + \text{M} \rightarrow \text{CH}_3\text{O}_2 + \text{M}$ $\text{CH}_3\text{O}_2 + \text{NO} \rightarrow \text{H}_3\text{CO} + \text{NO}_2$ $\text{H}_3\text{CO} + \text{O}_2 \rightarrow \text{H}_2\text{CO} + \text{HO}_2$ $\text{H}_2\text{CO} + \text{OH} \rightarrow \text{H}_2\text{O} + \text{HCO}$ $\text{HCO} + \text{O}_2 \rightarrow \text{HO}_2 + \text{CO}$ $\text{CO} + \text{OH} \rightarrow \text{CO}_2 + \text{H}$ $\text{H} + \text{O}_2 + \text{M} \rightarrow \text{HO}_2 + \text{M}$ $3(\text{NO} + \text{HO}_2 \rightarrow \text{NO}_2 + \text{OH})$ $2(\text{NO}_2 + h\nu \rightarrow \text{NO} + \text{O}({}^3\text{P}))$ $\underline{2(\text{NO}_2 + \text{O}({}^3\text{P}) \rightarrow \text{NO} + \text{O}_2)}$ net: $\text{CH}_4 + 2\text{O}_2 \rightarrow 2\text{H}_2\text{O} + \text{CO}_2$				$\text{CH}_4 + \text{OH} \rightarrow \text{CH}_3 + \text{H}_2\text{O}$ $\text{CH}_3 + \text{O}_2 + \text{M} \rightarrow \text{CH}_3\text{O}_2 + \text{M}$ $\text{CH}_3\text{O}_2 + \text{NO} \rightarrow \text{H}_3\text{CO} + \text{NO}_2$ $\text{H}_3\text{CO} + \text{O}_2 \rightarrow \text{H}_2\text{CO} + \text{HO}_2$ $\text{H}_2\text{CO} + \text{OH} \rightarrow \text{H}_2\text{O} + \text{HCO}$ $\text{HCO} + \text{O}_2 \rightarrow \text{HO}_2 + \text{CO}$ $\text{NO} + \text{HO}_2 \rightarrow \text{NO}_2 + \text{OH}$ $2(\text{NO}_2 + h\nu \rightarrow \text{NO} + \text{O}({}^3\text{P}))$ $2(\text{HO}_2 + \text{O}({}^3\text{P}) \rightarrow \text{OH} + \text{O}_2)$ $\text{CO} + \text{OH} \rightarrow \text{CO}_2 + \text{H}$ $\underline{\text{H} + \text{O}_2 + \text{M} \rightarrow \text{HO}_2 + \text{M}}$ net: $\text{CH}_4 + 2\text{O}_2 \rightarrow 2\text{H}_2\text{O} + \text{CO}_2$

Found_PAP = 5.65×10^{10} , Shown_PAP = 4.04×10^{10} , Total_chem = 1.24×10^{11} .

TABLE A1.3H. 3g M5 METHANE LOSS

Oxidation CH ₃ OOH-d (24.5%)	Oxidation CH ₃ OOH-e (23.7%)	Oxidation H ₂ O ₂ -a (5.8%)	Oxidation H ₂ O ₂ -b (4.5%)	Oxidation H ₂ O ₂ -c (4.4%)
2(CH ₄ + O ^(1D)) → CH ₃ + OH	CH ₄ + O ^(1D) → CH ₃ + OH	CH ₄ + O ^(1D) → CH ₃ + OH	CH ₄ + O ^(1D) → CH ₃ + OH	CH ₄ + O ^(1D) → CH ₃ + OH
2(CH ₃ + O ₂ + M → CH ₃ O ₂ + M)	CH ₃ + O ₂ + M → CH ₃ O ₂ + M	CH ₃ + O ₂ + M → CH ₃ O ₂ + M	CH ₃ + O ₂ + M → CH ₃ O ₂ + M	CH ₃ + O ₂ + M → CH ₃ O ₂ + M
2(CO + OH → CO ₂ + H)	CH ₃ O ₂ + HO ₂ → CH ₃ OOH + O ₂	CO + OH → CO ₂ + H	CO + OH → CO ₂ + H	CO + OH → CO ₂ + H
2(H + O ₂ + M → HO ₂ + M)	2(H + O ₂ + M → HO ₂ + M)	H + O ₂ + M → HO ₂ + M	H + O ₂ + M → HO ₂ + M	CH ₃ O ₂ + NO → H ₃ CO + NO ₂
2(CH ₃ O ₂ + HO ₂ → CH ₃ OOH + O ₂)	NO + HO ₂ → NO ₂ + OH	CH ₃ O ₂ + NO → H ₃ CO + NO ₂	CH ₃ O ₂ + NO → H ₃ CO + NO ₂	H ₃ CO + O ₂ → H ₂ CO + HO ₂
2(O ^(3P) + O ₂ + M → O ₃ + M)	2(CO + OH → CO ₂ + H)	H ₃ CO + O ₂ → H ₂ CO + HO ₂	H ₃ CO + O ₂ → H ₂ CO + HO ₂	H ₂ CO + <i>hν</i> → HCO + H
2(O ₃ + <i>hν</i> → O ₂ + O ^(1D))	NO ₂ + <i>hν</i> → NO + O ^(3P)	HO ₂ + HO ₂ → H ₂ O ₂ + O ₂	HO ₂ + HO ₂ → H ₂ O ₂ + O ₂	HCO + O ₂ → HO ₂ + CO
<u>O₂ + <i>hν</i> → O^(3P) + O^(3P)</u>	O ^(3P) + O ₂ + M → O ₃ + M	NO ₂ + <i>hν</i> → NO + O ^(3P)	NO ₂ + <i>hν</i> → NO + O ^(3P)	NO ₂ + <i>hν</i> → NO + O ^(3P)
net: 2CH ₄ + 2CO + 3O ₂ → 2CH ₃ OOH + 2CO ₂	<u>O₃ + <i>hν</i> → O₂ + O^(1D)</u>	O ^(3P) + O ₂ + M → O ₃ + M	O ^(3P) + O ₂ + M → O ₃ + M	O ^(3P) + O ₂ + M → O ₃ + M
	net: CH ₄ + 2CO + 2O ₂ → CH ₃ OOH + 2CO ₂	O ₃ + <i>hν</i> → O ₂ + O ^(1D)	<u>O₃ + <i>hν</i> → O₂ + O^(1D)</u>	O ₃ + <i>hν</i> → O ₂ + O ^(1D)
		<u>H₂CO + <i>hν</i> → H₂ + CO</u>	net: CH ₄ + CO + 2O ₂ → H ₂ CO + H ₂ O ₂ + CO ₂	2(H + O ₂ + M → HO ₂ + M)
		net: CH ₄ + 2O ₂ → H ₂ O ₂ + H ₂ + CO ₂		2(HO ₂ + HO ₂ → H ₂ O ₂ + O ₂)
				net: CH ₄ + 3O ₂ → 2H ₂ O ₂ + CO ₂

Found_PAP = 7.26 × 10¹⁰, Shown_PAP = 4.57 × 10¹⁰, Total_chem = 1.24 × 10¹¹.

436

TABLE A1.3I. 1g M7 METHANE LOSS

Oxidation 2O ₂ -f (23.6%)	Oxidation 3O ₂ -b (14.5%)	Oxidation 3O ₂ -a (11.1%)	Oxidation 2O ₂ -h (7.3%)	Oxidation 2O ₂ -i (5.4%)
			CH ₄ + OH → CH ₃ + H ₂ O	CH ₄ + OH → CH ₃ + H ₂ O
			CH ₃ + O ₂ + M → CH ₃ O ₂ + M	CH ₃ + O ₂ + M → CH ₃ O ₂ + M
			CH ₃ O ₂ + NO → H ₃ CO + NO ₂	CH ₃ O ₂ + NO → H ₃ CO + NO ₂
			H ₃ CO + O ₂ → H ₂ CO + HO ₂	H ₃ CO + O ₂ → H ₂ CO + HO ₂
			CH ₃ O ₂ + HO ₂ → CH ₃ OOH + O ₂	NO ₂ + O ^(3P) → NO + O ₂
			NO ₂ + O ^(3P) → NO + O ₂	H ₂ CO + O ^(3P) → HCO + OH
			CH ₃ OOH + OH → CH ₃ O ₂ + H ₂ O	HCO + O ₂ → HO ₂ + CO
			H ₂ CO + O ^(3P) → HCO + OH	2(NO + HO ₂ → NO ₂ + OH)
			HCO + O ₂ → HO ₂ + CO	CO + OH → CO ₂ + H
			CO + OH → CO ₂ + H	H + O ₂ + M → HO ₂ + M
			H + O ₂ + M → HO ₂ + M	2(NO + HO ₂ → NO ₂ + OH)
			2(NO + HO ₂ → NO ₂ + OH)	2(NO ₂ + <i>hν</i> → NO + O ^(3P))
			2(NO ₂ + <i>hν</i> → NO + O ^(3P))	net: CH ₄ + 2O ₂ → 2H ₂ O + CO ₂
			net: CH ₄ + 2O ₂ → 2H ₂ O + CO ₂	

Found_PAP = 5.48 × 10¹⁰, Shown_PAP = 3.40 × 10¹⁰, Total_chem = 1.24 × 10¹¹.

TABLE A2. OZONE COLUMN IN DOBSON UNITS (DU) FOR THE 1g, 3g SCENARIOS CORRESPONDING TO THE VALUES PLOTTED IN FIGURE 4A, 4B AS A FUNCTION OF STELLAR EFFECTIVE TEMPERATURE (T_{EFF}) (K)

T_{eff}	Column O_3 (DU) (1g)	Column O_3 (DU) (3g)
5800	305	275
3800	239	158
3400	270	251
3100	85	16.6
2800	59	5.3
2500	32	—

Acknowledgments

This research has been partly supported by the Helmholtz Gemeinschaft (HGF) through the HGF research alliance “Planetary Evolution and Life.” F. Selsis and P. von Paris acknowledge support from the European Research Council (Starting Grant 209622: E3ARTHS).

Abbreviations

ADL, AD Leonis; CIR, column-integrated rates; HZ, habitable zone; PAP, Pathway Analysis Program; SE, super-Earth; TOA, top of atmosphere.

References

- Bean, J.L., Desert, J.-M., Kabarg, P., Stalder, B., Seager, S., Miller-Ricci Kempton, E., Berta, Z.K., Homeier, D., Walsh, S., and Seifahrt, A. (2011) The optical and near-infrared transmission spectrum of the super-Earth GJ1214b: further evidence for a metal-rich atmosphere. *Astrophys J* 743, doi:10.1088/0004-637X/743/1/92.
- Benestad, R.E., editor. (2006) *Solar Activity and Earth's Climate*, 2nd ed., Springer, Berlin.
- Bonfils, X., Delfosse, X., Udry, S., Forveille, T., Mayor, M., Perrier, C., Bouchy, F., Gillon, M., Lovis, C., Pepe, F., Queloz, D., Santos, N.C., Ségransan, D., and Bertaux, J.-L. (2013) The HARPS search for southern extrasolar planets XXXI. The M dwarf sample. *Astron Astrophys* 549:A109.
- Borucki, W.J., Koch, D.G., Batalha, N., Bryson, S.T., Caldwell, D.A., Christensen-Dalsgaard, J., Cochran, W.D., DeVore, E., Gautier, T.N., Geary, J.C., Gilliland, R., Gould, A., Howell, S.B., Jenkins, J.M., Latham, D.W., Lissauer, J.J., Marcy, G.W., Sasselov, D., Boss, A., Charbonneau, D., Ciardi, D., Kaltenegger, L., Doyle, L., Dupree, A.K., Ford, E.B., Fortney, J., Holman, M.J., Steffen, J.H., Mullally, F., Still, M., Tarter, J., Ballard, S., Buchhave, L.A., Carter, J., Christiansen, J.L., Demory, B.-O., Désert, J.-M., Dressing, C., Endl, M., Fabrycky, D., Fischer, D., Haas, M.R., Henze, C., Horch, E., Howard, A.W., Isaacson, H., Kjeldsen, H., Johnson, J.A., Klaus, T., Kolodziejczak, J., Barclay, T., Li, J., Meibom, S., Prsa, A., Quinn, S.N., Quintana, E.V., Robertson, P., Sherry, W., Shporer, A., Tenenbaum, P., Thompson, S.E., Twicken, J.D., Van Cleve, J., Welsh, W.F., Basu, S., Chaplin, W., Miglio, A., Kawaler, S.D., Arentoft, T., Stello, D., Metcalfe, T.S., Verner, G.A., Karoff, C., Lundkvist, M., Lund, M.N., Handberg, R., Elsworth, Y., Hekker, S., Huber, D., Bedding, T.R., and Rappin, W. (2012) Kepler-22b a 2.4 Earth-radius planet in the habitable zone of a Sun-like star. *Astrophys J* 745, doi:10.1088/0004-637X/745/2/120.
- Brasseur, G. and Solomon, S., editors. (2005) *Aeronomy of the Middle Atmosphere: Chemistry and Physics of the Stratosphere and Mesosphere*, Springer Press, Dordrecht.
- Chameides, W.L., Stedman, D.H., Dickerson, R.R., Rusch, D.W., and Ciccone, R.J. (1977) NOx production in lightning. *Journal of the Atmospheric Sciences* 34:143–149.
- Chapman, S.A. (1930) Theory of upper-atmospheric ozone. *Memoirs of the Royal Meteorological Society* 3:103–125.
- Chemical Rubber Company (CRC). (1976) *CRC Handbook of Chemistry and Physics: A Ready-Reference Book of Chemical and Physical Data*, 57th ed., CRC Press, Cleveland, OH.
- Croll, B., Albert, L., Jayawardana, R., Miller-Ricci Kempton, E., Fortney, J.J., Murray, N., and Neilson, H. (2011) Broadband transmission spectroscopy of the super-Earth GJ1214b suggests a low mean molecular weight atmosphere. *Astrophys J* 736, doi:10.1088/0004-637X/736/2/78.
- Crutzen, P.J. (1970) The influence of nitrogen oxides on the atmospheric ozone content. *Quarterly Journal of the Royal Meteorological Society* 96:320–325.
- Elkins-Tanton, E. and Seager, S. (2008) Ranges of atmospheric mass and composition for super-Earth exoplanets. *Astrophys J* 685:1237–1246.
- Estupiñan, E.G., Nicovich, J.M., Li, D., Cunnold, D.M., and Wine, P.H. (2002) Investigation of N₂O production from 266 and 532 nm laser flash photolysis of O₃/N₂/O₂ mixtures. *J Phys Chem A* 106:5880–5890.
- Fast, K.E., Kostiuk, T., Lefevre, F., Hewagama, T., Livengood, T.A., Delgado, J.D., Annen, J., and Sonnabend, G. (2009) Comparison of HIPWAC and Mars Express SPICAM observations of ozone on Mars 2006–2008 and variation from 1993 IRHS observations. *Icarus* 203:20–27.
- France, K., Froning, C.S., Linsky, J.L., Roberge, A., Stocke, J.T., Tian, F., Bushinsky, R., Désert, J.-M., Mauas, P., Vieytes, M., and Walkowicz, L.M. (2013) The ultraviolet radiation environment around M-dwarf exoplanet host stars. *Astrophys J* 763, doi:10.1088/0004-637X/763/2/149.
- Grenfell, J.L., Savage, N.H., Harrison, R.M., Penkett, S.A., Forberich, O., Comes, F.J., Clemitshaw, K.C., Byrgess, R.A., Cardenas, L.M., Davison, B., and McFadyen, G.G. (1999) Tropospheric box-modelling and analytical studies of the hydroxyl (OH) radical and related species: comparison with observations. *J Atmos Chem* 33:185–217.
- Grenfell, J.L., Lehmann, R., Mieth, P., Langematz, U., and Steil, B. (2006) Chemical reactions pathways affecting stratospheric and mesospheric ozone. *J Geophys Res* 111, doi:10.1029/2004JD005713.
- Grenfell, J.L., Stracke, B., von Paris, P., Patzer, B., Titz, R., Segura, A., and Rauer, H. (2007) The response of atmospheric chemistry on Earth-like planets around F, G and K stars to small variations in orbital distance. *Planet Space Sci* 55: 661–671.
- Guenther, E.W., Cabrera, J., Erikson, A., Fridlund, M., Lammer, H., Mura, A., Rauer, H., Schneider, J., Tulej, M., von Paris, P., and Wurz, P. (2011) Constraints on the exosphere of CoRoT-7b. *Astron Astrophys* 525:A24.
- Gueymard, C. (2004) The Sun's total and spectral irradiance for solar energy applications and solar radiation models. *Solar Energy* 76:423–453.
- Haagen-Smit, A.J. (1952) Chemistry and physiology of Los Angeles Smog. *Ind Eng Chem* 44:1342–1346.
- Hawley, S. and Pettersen, B.R. (1991) The great flare of 1985 April 12 on AD Leonis. *Astrophys J* 378:725–741.
- Houghton, J.T., Ding, Y., Griggs, D.J., Noguier, M., van der Linden, P.J., Dai, X., Maskell, K., and Johnson, C.A., editors.

- (2001) *Climate Change 2001: The Scientific Basis*, Contribution of Working Group I to the Third Assessment Report of the Intergovernmental Panel on Climate Change (IPCC), Cambridge University Press, Cambridge, UK.
- Jucks, K.W., Johnson, D.G., Chance, K.V., and Traub, W.A. (1996) Ozone production and loss rate measurements in the middle stratosphere. *J Geophys Res* 101:28785–28792.
- Keppler, F., Harper, D.B., Röckmann, T., Moore, R.M., and Hamilton, J.T.G. (2005) New insight into the atmospheric chloromethane budget gained using stable carbon isotope ratios. *Atmos Chem Phys* 5:2403–2411.
- Lehmann, R. (2004) An algorithm for the determination of all significant pathways in chemical reaction systems. *J Atmos Chem* 47:45–78.
- Lielieveld, J., Peters, W., Dentener, F.J., and Krol, M.C. (2002) Stability of tropospheric hydroxyl chemistry. *J Geophys Res* 107, doi:10.1029/2002JD002272.
- Mayor, M., Bonfils, X., Forveille, T., Doflosse, X., Udry, S., Bertriaux, J.-L., Beust, H., Bouchy, F., Lovis, C., Pepe, F., Perrier, C., Queloz, D., and Santos, N.C. (2009) The HARPS search for southern extra-solar planets. An Earth-mass planet in the GJ 581 planetary system. *Astron Astrophys* 507:487–494.
- Montmessin, F., Bertriaux, J.-L., Lefevre, F., Marcq, E., Belyaev, D., Gerard, J.-C., Korablev, O., Fedorova, A., Sarago, V., and Vandaele, A.C. (2011) A layer of ozone detected in the nightside upper atmosphere of Venus. *Icarus* 216:82–85.
- Muirhead, P.S., Johnson, J.A., Apps, K., Carter, J.A., Morton, T.D., Fabrycky, D.C., Pineda, J.S., Bottom, M., Rojas-Ayala, B., Schlawin, E., Hamren, K., Covey, K.R., Crepp, J.R., Stassun, K.G., Pepper, J., Hebb, L., Kirby, E.N., Howard, A.W., Isaacson, H.T., Marcy, G.W., Levitan, D., Diaz-Santos, T., Armus, L., and Lloyd, J.P. (2012) Characterizing the cool KOIs. III. KOI 961: a small star with large proper motion and three small planets. *Astrophys J* 747, doi:10.1088/0004-637X/747/2/144.
- NASA Panel for Data Evaluation. (2003) *Chemical Kinetics and Photochemical Data for Use in Atmospheric Studies*, Evaluation No. 14, JPL Publication 02-25, Jet Propulsion Laboratory, Pasadena, CA.
- Rauer, H., Gebauer, S., v. Paris, P., Cabrera, J., Godolt, M., Grenfell, J.L., Belu, A., Selsis, F., Hedelt, P., and Schreier, F. (2011) Potential biosignatures in super-Earth atmospheres I. Spectral appearance of super-Earths around M-dwarfs. *Astron Astrophys* 529:A8.
- Reiners, A., Joshi, N., and Goldman, B. (2012) A catalogue of rotation and activity in early M-stars. arXiv:1201.5774v1.
- Savage, N.H., Harrison, R.M., Monks, P.S., and Salisbury, G. (2001) Steady-state modelling of radical concentrations at Mace Head during the EASE'97 campaign, May, 1997. *Atmos Environ* 35:515–524.
- Schumann, U. and Huntreiser, H. (2007) The global lightning-induced nitrogen oxides source. *Atmos Chem Phys* 7:3823–3907.
- Segura, A., Krellove, K., Kasting, J.F., Sommerlatt, D., Meadows, V., Crisp, D., Cohen, M., and Mlawer, E. (2003) Ozone concentrations and ultraviolet fluxes on Earth-like planets around other stars. *Astrobiology* 3:689–708.
- Segura, A., Kasting, J.F., Meadows, V., Cohen, M., Scalo, J., Crisp, D., Butler, R.A.H., and Tinetti, G. (2005) Biosignatures from Earth-like planets around M dwarfs. *Astrobiology* 5: 706–725.
- Segura, A., Meadows, V., Kasting, J.F., Crisp, D., and Cohen, M. (2007) Abiotic formation of O₂ and O₃ in high-CO₂ terrestrial atmospheres. *Astrobiology* 472:665–679.
- Selsis, F., Despois, D., and Parisot, J.-P. (2002) Signature of life on exoplanets—can Darwin produce false detections? *Astron Astrophys* 388:985–1003.
- Stamenković, V., Noack, L., Breuer, D., and Spohn, T. (2012) The influence of pressure-dependent viscosity on the thermal evolution of super-Earths. *Astrophys J* 748, doi:10.1088/0004-637X/748/1/41.
- Stock, J., Grenfell, J.L., Lehmann, R., Patzer, A.B.C., and Rauer, H. (2012a) Chemical pathway analysis of the lower martian atmosphere: the CO₂ stability problem. *Planet Space Sci* 68: 18–24.
- Stock, J., Boxe, C.S., Lehmann, R., Grenfell, J.L., Patzer, A.B.C., Rauer, H., and Yung, Y.L. (2012b) Chemical pathway analysis of the martian atmosphere: CO₂-formation pathways. *Icarus* 219:13–24.
- Toon, O.B., McKay, C.P., Ackerman, T.P. and Santhanam, K. (1989) Rapid calculation of radiative heating rates and photodissociation rates in inhomogeneous multiple scattering atmospheres. *J Geophys Res* 94:16287–16301.
- Udry, S., Bonfils, X., Delfosse X., Forveille, T., Mayor, M., Perrier, C., Bouchy, F., Lovis, C., Pepe, F., Queloz, D., and Bertriaux, J.-L. (2007) The HARPS search for southern extra-solar planets—XI. Super-Earths (5 and 8 M_⊕) in a 3-planet system. *Astron Astrophys* 469:L43–L47.
- Walkowicz, L.M., Johns-Krull, C.M., and Hawley, S.L. (2008) Characterising the near-UV environment of M dwarfs. *Astrophys J* 677:593–606.
- Wang, P., Li, Z., Cihlar, J., Wardle, D.I., and Kerr, J. (2000) Validations of an UV inversion algorithm using satellite and surface measurements. *J Geophys Res* 105:5037–5058.
- Whalley, L.K., Furneaux, K.L., Goddard, A., Lee, J.D., Mahajan, A., Oetjen, H., Read, K. A., Kaaden, N., Carpenter, L.J., Lewis, A.C., Plane, J.M.C., Saltzman, E.S., Wiedensohler, A., and Heard, D.E. (2010) The chemistry of OH and HO₂ radicals in the boundary layer over the tropical Atlantic Ocean. *Atmos Chem Phys* 10:1555–1576.
- WMO. (1995) *Scientific Assessment of Ozone Depletion: 1994*, Global Ozone Research and Monitoring Project—Report No. 37, National Oceanic and Atmospheric Administration, National Aeronautics and Space Administration, United Nations Environment Programme, and World Meteorological Organization (WMO).

Address correspondence to:

J.L. Grenfell
DLR—German Aerospace Centre
Institute of Planetary Research
Berlin, Germany

E-mail: lee.grenfell@dlr.de

Submitted 8 October 2012
Accepted 19 February 2013